~~Enhanced isotopic approach combined with microbiological analyses for more precise distinction of various N-transformation processes in contaminated aquifer – a groundwater incubation study~~

N-transformations in nitrate-rich groundwaters: combined isotope and microbial approach

Sushmita Deb[1], Mikk Espenberg[2], Reinhard Well[3], ~~Ülo Mander[2]~~, Michał Bucha[1], Marta Jakubiak[1], Ülo Mander[2], Mariusz-Orion Jędrysek[1], Dominika Lewicka-Szczebak[1]

[1] Institute of Geological Sciences, University of Wrocław, Poland
[2] Institute of Ecology and Earth Sciences, University of Tartu, Estonia
[3] Thünen Institute of Climate-Smart Agriculture, Braunschweig, Germany

Correspondence to: Sushmita Deb (sushmita.deb@uwr.edu.pl)

Abstract

This study explores nitrogen transformations in groundwater from an agricultural area utilizing organic fertilizer (wastewaters from yeast production) by integrating ~~isotopic~~isotope analysis, microbial gene abundance, and the FRAME (isotope FRactionation And Mixing Evaluation) model to trace and quantify nitrogen cycling pathways. Groundwater samples with elevated nitrate concentrations were subjected to controlled laboratory incubations with application of a novel low-level ^{15}N tracing strategy, to investigate microbial processes. Isotope analyses of nitrate, nitrite and nitrous oxide (N_2O), coupled with microbial gene quantification via quantitative PCR (qPCR), revealed a shift from archaeal-driven nitrification to bacterial denitrification in post-incubation suboxic conditions, stimulated by glucose addition. FRAME modeling further identified bacterial denitrification ~~(bD)~~ as the dominant pathway of N_2O production, which was supported by increased *nosZI, nirK and nirS* gene abundance and observed isotope effects.

Simultaneously to the intensive nitrate reduction, it was observed that the majority of nitrite is likely produced through nitrification processes linked to dissolved organic nitrogen (DON) oxidation. Nitrate reduction had minor contribution in the total nitrite pool. The results demonstrate the efficacy of integrating multi-compound isotope studies and microbial analyses to unravel nitrogen cycling mechanisms. This approach provides a robust framework for addressing nitrogen pollution in groundwater systems and improving water quality management strategies.

Introduction

43 Nitrogen (N) is an essential nutrient for plant growth and global food production, forming a key
44 component of nucleic acids and proteins. Although synthetic N fertilizers containing nitrate (NO_3^-)
45 and/or ammonium (NH_4^+), have greatly influenced agricultural yields, their excessive use has
46 significantly disrupted the N cycle, leading to NO_3^- leaching in groundwater, emission of ammonia
47 (NH_3), and gaseous forms of nitrogen oxides (nitric oxide (NO), nitrous oxide (N_2O), nitrogen
48 dioxide (NO_2~~)~~)) which are of environmental concern (Sainju et al., 2020). ~~These~~ ~~issues~~N-
49 compounds contribute to eutrophication of ~~lakes~~surface waters, groundwater quality degradation,
50 and greenhouse ~~gas emissions~~effect, with N_2O intensifying global warming and ozone depletion
51 (Butterbach-Bahl et al., 2013). Controlling NO_3^- levels in aquatic systems presents substantial
52 environmental challenges, particularly in groundwater, due to the complexity of differentiating
53 between its anthropogenic sources ~~and natural processes.~~- such as fertilizer runoff, waste from
54 livestock manure, industrial wastewater discharges - and natural processes including soil organic
55 matter mineralization, precipitation and biological nitrogen fixation by microorganisms. Also,
56 nitrite (NO_2^-), a transient intermediate in the nitrogen cycle, can accumulate under certain
57 environmental conditions and pose significant environmental and health risks such as
58 methemoglobinemia (blue baby syndrome) in infants and carcinogenic nitrosamines (Ward et al.,
59 2018). Further, elevated NO_2^- levels in water bodies and agricultural soils, can be toxic to aquatic
60 life and humans, and therefore underscore the importance of monitoring NO_2^- alongside NO_3^- in
61 groundwater systems. Hence, the better understanding of N cycling is crucial to develop effective
62 solutions of environmental problems (Rütting et al., 2018).

64 Diverse microbial communities, including nitrogen-fixing bacteria, archaea, anammox bacteria,
65 nitrifiers, and denitrifiers, drive key N transformations, regulating its availability and mobility in
66 ecosystems. N undergoes complex transformation processes like nitrification, denitrification,
67 anammox, mineralization and immobilization (Deb et al., 2024) which regulate N availability to
68 plants and influence its movement in agricultural and natural systems. Biological fixation converts
69 atmospheric nitrogen (N_2) into bioavailable forms, while nitrification involves the microbial
70 oxidation of NH_4^+ to NO_3^- via ~~nitrite (NO_2^-).~~$_2^-$. Denitrification reduces NO_3^- to N_2 through the
71 intermediates NO_2^-, NO and N_2O. Depending on environmental conditions, this reduction may be
72 incomplete, leading to N_2O emissions. Moreover, the anammox or feammox processes converts of
73 NH_4^+ and NO_2^- to N_2 (Ding et al., 2022; Einsiedl et al., 2020). These processes are interconnected
74 and influenced by environmental conditions, making it challenging to differentiate between the
75 sources and pathways of N transformations (Nikolenko et al., 2018). ~~Further, functional~~
76 ~~characterization of genes encoding key enzymes in N metabolism provides insights into the genetic~~
77 ~~potential for specific transformations (Levy-Booth et al., 2014), while microbial community~~
78 ~~structure analysis helps elucidate the physiological activities and ecological roles of microbes in~~
79 ~~driving N transformations. Together, these approaches contribute to a comprehensive~~
80 ~~understanding of N cycling processes.~~

82 Stable isotope studies help in tracing the N sources and transformations, through isotopic
83 signatures such as $\delta^{15}N$ and $\delta^{18}O$ in NO_3^-, NO_2^-, NH_4^+, and N_2O (including ^{15}N site preference in
84 the linear N_2O molecule ($\delta^{15}N^{SP}$)) (Denk et al., 2017, Deb et al., 2024). However, limitations arise
85 due to overlapping ranges of different isotope sources or difficulty in distinction between isotope
86 fractionation processes and mixing. To overcome such limitations and enhance interpretations
87 based on stable isotope studies a multi-compound analysis approach can be applied (Well et al.,
88 2012, Deb et al., 2024). Such ~~multi-compound isotope analysis~~approach provides a broader

89 perspective on N cycle processes by examining multiple N-compounds e.g., in denitrification δ^{15}N
90 and δ^{18}O analysis of NO_3^- helps identify substrates, while NO_2^- and N_2O analyses provide insight
91 into intermediate products.
92 ~~Since~~However, since the range of natural isotope variations is relatively narrow, even analyses of
93 multiple compounds may provide ambiguous results. ^{15}N tracing technique allows ~~for precise~~
94 ~~tracing of~~ to track precisely the artificially added N in the environment (Müller et al., 2004~~)~~), but
95 is spatially and temporally limited and disrupts natural abundance isotope studies (Buchen-
96 Tschiskale et al., 2023; Well et al., 2019)~~,~~, which are easily and universally applicable in
97 unmodified environmental conditions. A major drawback of traditional ^{15}N tracing methods is the
98 necessary sacrifice of other isotope tracers, such as O isotope signatures and site preference values
99 of N_2O, which cannot be accurately determined when high ^{15}N additions are applied. This research
100 introduces a novel approach using low-level ^{15}N labelling, where a minimal amount of ^{15}N-labelled
101 substrate is added to slightly increase δ^{15}N values (up to ca. 100-200‰) of a single substrate while
102 maintaining the natural abundance levels. This ensures that isotope fractionation remains relevant,
103 and standard measurement methods for all isotope signatures can still be applied. If the level of
104 the applied ^{15}N labelling exceeds the natural variability of N sources and isotope fractionation
105 effects, this approach enables clear distinction between substrates involved in N transformations.
106 It also allows for precise tracing of the path of N from substrate to product while simultaneously
107 utilizing or determining isotope fractionation factors~~,~~. In consequence, such low-labelling
108 experiments are directly relevant and comparable to the field conditions. Moreover the needed
109 addition of N to the system is minimal which ~~remain applicable to natural abundance isotope~~
110 ~~studies in natural environments~~allows to avoid the effect of additional fertilization of the system
111 under study.
112 While stable isotope analysis provides valuable insights into nitrogen pathways, its interpretation
113 is often complicated by overlapping fractionation effects (Deb et al., 2024). To refine process
114 identification, microbiological approaches ~~such as~~can be applied. Functional characterization of
115 genes encoding key enzymes in N metabolism provides insights into the genetic potential for
116 specific transformations (Levy-Booth et al., 2014), while microbial community structure analysis
117 helps elucidate the physiological activities and ecological roles of microbes in driving N
118 transformations and quantitative PCR (qPCR) enable the ~~detection and~~ quantification of ~~key genes~~
119 ~~involved in nitrogen transformations, providing insights into~~ particular genes and hence
120 assessment of their microbial activity (Espenberg et al., 2018; Rohe et al., 2020). Together, these
121 approaches contribute to a comprehensive understanding of N cycling processes.
122
123 However, these microbiological methods only reveal the potential for microbial species to
124 participate in nitrogen cycling rather than directly quantifying transformation rates. The detection
125 of functional genes or gene expression does not confirm whether a process is actively occurring at
126 a given time or its relative contribution within a system (Espenberg et al., 2018; Rohe et al., 2020).
127 Thus, combining stable isotope data with microbiological analyses enhances the precision of
128 nitrogen flux assessments in groundwater, offering a robust framework for tracing, quantifying,
129 and characterizing nitrogen transformations in complex environmental systems. The integration of
130 isotopic and microbial techniques for partitioning N cycle processes provided so far valuable
131 insights into N_2O source apportioning (Masta~~(MASTA~~ et al., 2024).
132 Here we combine the isotope studies, applying novel low-labelling technique and
133 ~~multicompound~~multi-compound isotope analyses, with microbiological analyses using
134 quantitative PCR (qPCR), which identify and quantify key genes involved in N processes. This

135 aims at better understanding of the occurring N transformations and enhancement the precision of
136 nitrogen flux assessments in groundwater.
137

2. Materials and Methods

2.1. Experimental Site

Experiments were conducted from the groundwaters collected in an agricultural area near Wołczyn, Poland, approximately 80 km north of Wrocław. On these crop fields wastewater from a yeast factory is applied as a natural fertilizer, containing 300 mg L^{-1} of TN (total nitrogen) and 835 mg L^{-1} of TP (total potassium). While this approach supports agricultural production by reducing reliance on synthetic fertilizers, it is likely to have a significant impact on groundwater quality, especially by increasing N and P load. Preliminary sampling from piezometers in the study area conducted on July 2023 revealed nitrate concentrations exceeding 80 mg L^{-1} in the groundwater, raising concerns about elevated nitrate levels, exceeding the norms for drinking water of 50 mg L^{-1}. The following map (Fig. 1) illustrates the study area of our experiment, highlighting the locations of piezometers used for groundwater sampling.
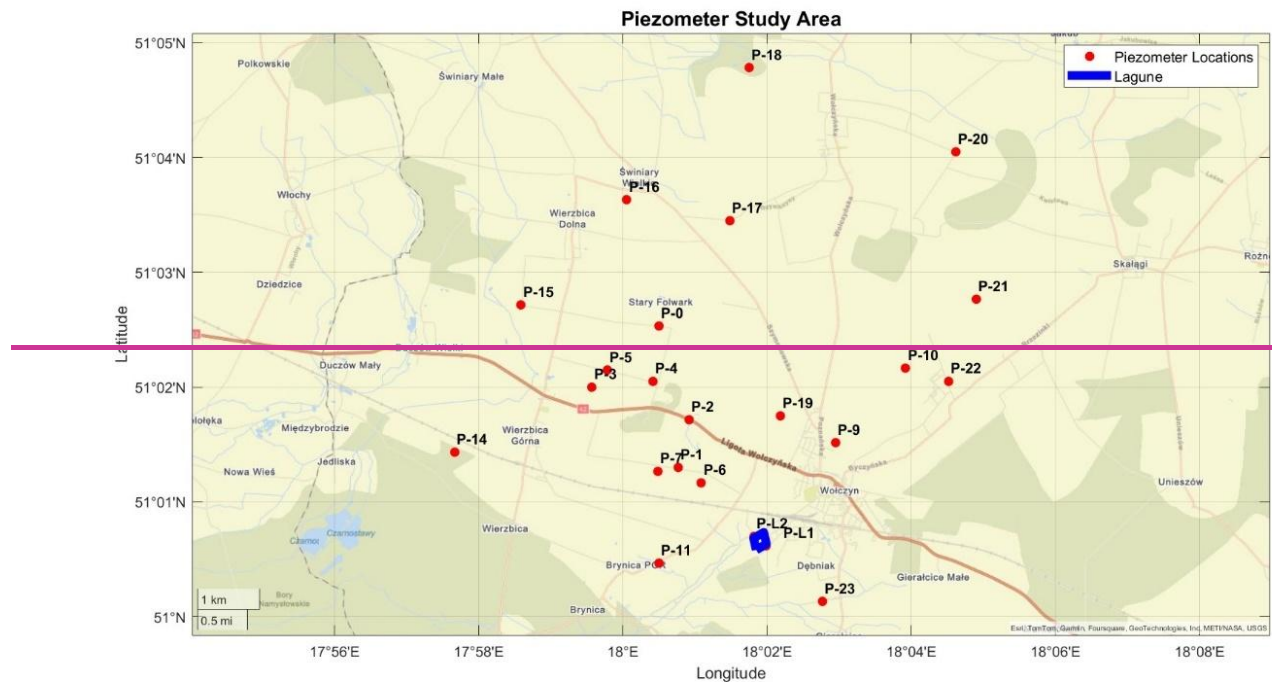

Figure 1: Piezometer Study Area near Wołczyn, Poland (~~Blue~~Purple-marked area indicates the lagune for yeast-production sewage storage).

The aquifer under study is the top first groundwater horizon connected with surface waters, built of sand-gravel formations of Neogene-Quaternary, hydraulically separated from the underlying Triassic horizon by shale layers. The water table has unconfined character and varying depths from 1.5 to 18.7 m below surface (Olichwer et al., 2012). The thickness of the aquifer range from 4.5 to 31.9 m. The redox potential of the sampled groundwaters varies from 213 to 345 mV and dissolved O_2 concentration from 2.2. to 4.3 mg dm^{-3}. These values indicate lower O_2 content when combinedcompared to saturated conditions (ca. 10 mg dm^{-3}), but slightly higher than typical denitrification favoring conditions (below 2 mg dm^{-3}) (Wolters et al., 2022). The dissolved O_2 range provided here reflects typical suboxic conditions in this aquifer system, as reported in previous field campaigns in the Wołczyn region (Olichwer et al., 2012). In the present study, individual dissolved O_2 concentrations were not systematically recorded for each piezometer due to unexpected problems, and thus, the cited range serves as a general background representation of aquifer conditions.

2.2. Water Sampling

Groundwater samples from 23 piezometers in the study area were pumped out at varying depths during the field sampling campaign on 5th September 2023 (Table 1S1). Subsequently, water from four selected piezometers (P-7, P-16, P-20, P-23) with high nitrate concentrations were used for laboratory incubation studies to evaluate the potential N transformation processes and to identify the isotope effects associated with them. Although P-0 and P-3 also exhibited comparably high nitrate concentration levels, they were excluded from the incubation experiments due to limited water availability at the time of sampling.

Table 1: Concentrations of Nitrogen Species and Environmental Parameters in Groundwater Samples (P abbreviated for piezometer), bd – below detection, piezometers selected for incubation – in bold font.

Sample	Temperature (°C)	pH	Conductivity (µS cm^{-1})	Nitrate (N-NO$_3^-$) (mg N L^{-1})	Nitrite (N-NO$_2^-$) (mg N L^{-1})	Ammonium (N-NH$_4^+$) (mg N L^{-1})	DOC (dissolved organic carbon) (mg C L^{-1})	DON (dissolved organic nitrogen) (mgN L^{-1})	δ^{15}N		δ^{18}O	
									δ^{15}N-NO$_3^-$	δ^{15}N-NO$_2^-$	δ^{18}O-NO$_3^-$	δ^{18}O-NO$_2^-$
P-0	13.5	6.5	928	39.65	0.08	0.33	24.12	32.76	0.9	-31.0	0.5	bd
P-1	14	6.1	1000	21.05	0.284	0.224	42.06	16.76	7.7	-27.8	6.1	-7.3
P-2	13.4	7.3	1245	0.62	0.21	7.05	67.42	bd	bd	bd	bd	bd
P-3	14.1	6.7	998	39.3	0.405	0.316	27.28	57.08	4.3	-30.2	0.4	-4.2
P-4	12.8	7.3	4794	0.63	0.398	11.46	431.3	7.74	bd	bd	bd	bd
P-5	13.5	6.8	1030	18.45	0.092	0.103	176.9	6.12	9.3	bd	3.3	bd

P-6	17	7.5	1386	0.24	0.034	0.31	58.42	bd	bd	bd	bd	bd
P-7	13.2	6.9	1395	32.8	0.188	0.138	46.32	41.04	6.6	-37.0	3.2	8.5
P-9	14.4	6.7	919	0.11	<0	0.17	52.59	bd	bd	bd	bd	bd
P-10	12.2	6.8	944	0.98	0.02	1.509	24.66	bd	10.4	bd	6.1	bd
P-11	14.2	7.3	1343	0.5	0.081	2.33	bd	bd	bd	bd	bd	bd
P-14	15.5	7.1	845	0.33	0.114	14.98	bd	bd	bd	bd	bd	bd
P-15	14.7	7	512	0.44	0.146	4.397	22.28	bd	bd	bd	bd	bd
P-16	10	6.2	617	39.45	0.098	0.031	10.22	31.88	3.7	-17.3	1.6	4.4
P-17	12.7	7.1	685	0.26	0.018	0.557	51.81	bd	bd	bd	bd	bd
P-18	11.2	7.1	560	1.8	0.06	0.651	55.85	bd	8.4	bd	7.7	bd
P-19	13.9	6.6	617	0.52	0.025	0.611	9.23	bd	bd	bd	bd	bd
P-20	11.1	6.6	471	38.12	0.019	0.028	9.7	30.63	1.0	bd	-0.9	bd
P-21	10.9	7.1	574	0.43	0.087	0.565	31.49	bd	bd	bd	bd	bd
P-22	11.1	5.6	557	2.47	0.064	0.215	14.81	5.01	16.0	bd	4.8	bd
P-23	14.9	6.3	1238	89.5	0.354	0.059	21.22	91.72	5.3	-27.9	4.7	-8.9
P-L1	14.2	6.8	2581	1.26	0.226	0.817	262.4	69.28	10.3	5.4	1.9	15.7
P-L2	13.8	7	1777	0.2	0.058	17.95	68.9	25.74	bd	bd	bd	bd
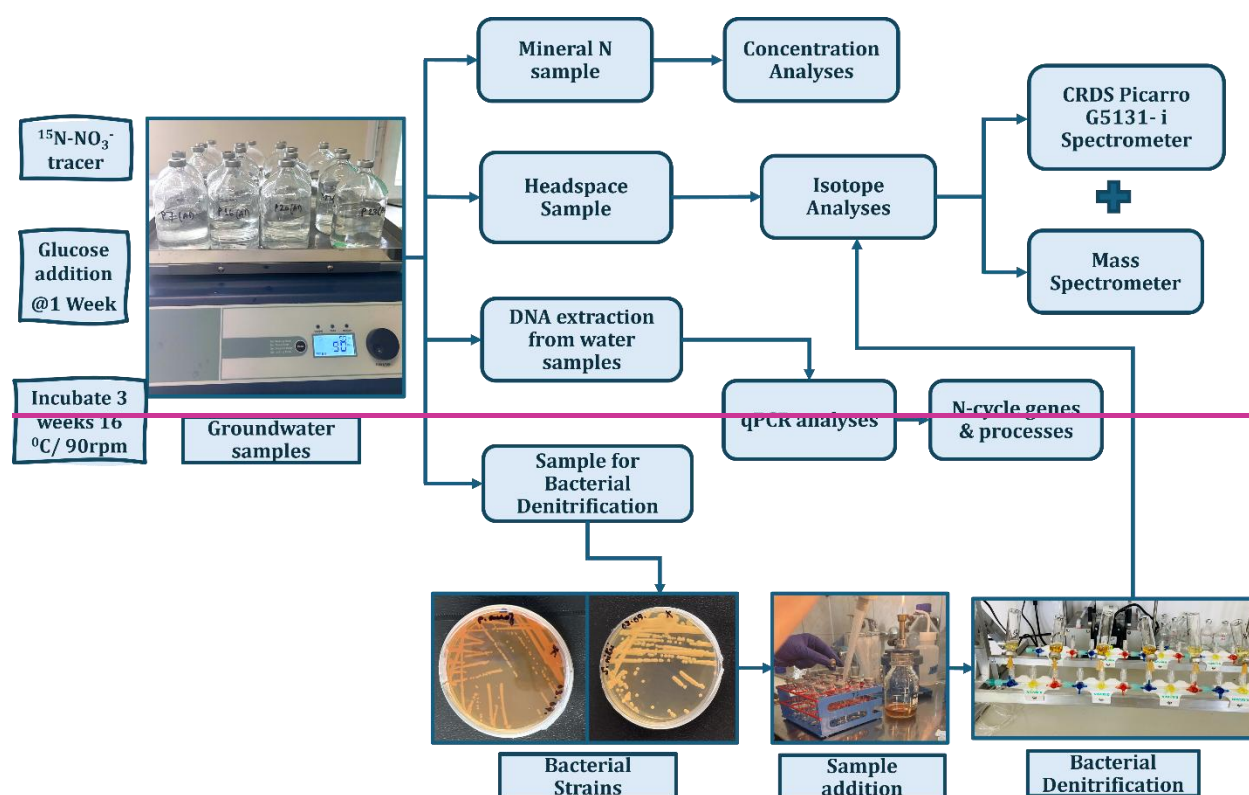
187

$^{15}N\text{-}NO_3^-$ tracer

Glucose addition @1 Week

Incubate 3 weeks 16 °C/ 90rpm

Groundwater samples

Mineral N sample → Concentration Analyses

Headspace Sample → Isotope Analyses → CRDS Picarro G5131- i Spectrometer + Mass Spectrometer

DNA extraction from water samples

qPCR analyses → N-cycle genes & processes

Sample for Bacterial Denitrification

Bacterial Strains

Sample addition

Bacterial Denitrification

Figure 2: Experimental Setup for microbial analyses (qPCR, Groundwater Incubation) and Isotopic Analysis. The scheme illustrates the workflow for analyzing groundwater samples, including incubation with $^{15}N\text{-}NO_3^-$ tracer, bacterial denitrification, DNA extraction, concentration analyses, and isotope measurements using a CRDS (Cavity Ring Down Spectroscopy) Picarro G5131-i spectrometer and mass spectrometer.

For inorganic N concentration and isotopic analyses, all groundwater samples were filtered using 0.45 μm filters. For NO_3^- and NH_4^+ analysis, 50 ml of the filtered sample was collected in a Falcon tube, which was stored frozen until further analysis. For NO_2^- analysis, an additional 50 ml of the sample was collected in a separate Falcon tube, where after filtering 1 mL of 2 M KOH was added to raise the pH to 10-12, inhibiting ~~nitrite~~NO_2^- reduction. The samples were then stored at 4 °C until further analysis. It is essential to analyze these samples as soon as possible after collection to prevent microbial degradation and ensure data integrity.

From the field sampling ~~4~~the four selected samples ~~with high nitrate concentration~~ were used for filtering and further microbial analyses. The field groundwater samples were immediately

7

transported to the laboratory in an ice-cooled box and filtered using 0.45 μm filters-. For laboratory incubation studies, 2 ltL of groundwater from selected piezometers with high nitrate concentration were collected into sterile bottles and immediately sealed for a series of laboratory experiments, and stored frozen until further analysis. -Further, from the later incubation studies (as described in 2.52), the water samples (600 ml from each incubated piezometers) were filtered using sterile 0.45 μm filters for the further microbial analyses after the 3 week incubations period- (Fig.2).

2.3. Laboratory incubation of groundwater samples

Laboratory incubation studies were conducted with groundwater samples from four selected piezometers (P, abbreviated for piezometer: P-7, P-16, P-20, and P-23) with high NO_3^- concentrations to investigate natural NO_3^- reduction and identify favorable conditions for denitrification. Due to restricted water availability in some piezometers, where the aquifer was quickly pumped out and the water amount required for the further incubations (min. 1500 mL) could not be collected, some potentially interesting piezometers must have been omitted. This was the case for e.g. P-0 and P-3 where despite high NO_3^- concentrations the incubations were not possible due to too little water gain.

A volume of 150 mL of groundwater from each piezometer was transferred into sterile 250 mL flasks, with each sample prepared in four replicates along with sterile controls. Sterile samples were produced by filtering the groundwater through 0.45 μm filters followed by the addition of 2 mL of $HgCl_2$ to inhibit microbial activity. These sterile samples served as controls for comparison with active treatments. The incubation flasks with groundwater samples were flushed with N_2 gas for 15 minutes, with the flow rate 60–70 mL min^{-1} and 0.6 Bar, to create suboxic conditions of similar O_2 content as in the studied aquifer. The final O_2 concentration in the headspace was about 5%, which corresponds to the dissolved O_2 content in water of 2.1 mg L^{-1} (Table S2). The pH of the samples, approximately 6.5 for each, was maintained without any adjustments. Prior to incubation, a low amount of $^{15}N-NO_3^-$ labelled tracer was added to each sample based on its initial nitrate concentration resulting in at% ^{15}N (Atom Percent ^{15}N) of 0.4296%–0.4700%, slightly exceeding the natural abundance (0.366%), to trace N transformation pathways. The target $\delta^{15}N$ value of final NO_3^- was 200‰. A stock solution was prepared by dissolving 12.1429 mg of $Na^{15}NO_3$ (99% ^{15}N) in 50 mL of water. From this, 1 mL was added to samples P-7, P-16, and P-20, while 2 mL was added to P-23. The added volume of ^{15}N-labelled tracer solution was adjusted according to the nitrate concentration in each sample to achieve a comparable level of isotopic enrichment across all samples while minimizing alteration to the natural isotopic composition. Further, 1 mL of glucose, equivalent to the addition of 616 mg of C, was added as an additional carbon source after one week of incubation to additionally stimulate microbial activity and enhance denitrification. All samples were incubated in dark for three weeks at 16 °C with agitation at 90 rpm.

2.3Inorganic N compounds in incubated samples were analyzed at the beginning, after one week of incubation before glucose addition, and at the end of the experiment for their concentration (section 2.4) and isotope signatures (section 2.5). The gas headspace samples were collected every second day and analysed for N_2O and CO_2 concentration and N_2O isotope signatures (section 2.6).

8

2.4. Inorganic nitrogen analyses (NO$_3^-$, NO$_2^-$, NH$_4^+$) Using a Colorimetric Method

For the analysis of NO$_3^-$, NO$_2^-$, and NH$_4^+$ concentrations, groundwater samples were filtered using 0.45 μm filters and measured with the SLANDI Photometer LF300 (Slandi Sp. z o.o., Michałowice, Poland), a versatile instrument for water and wastewater analysis across wavelengths ranging from 380 nm to 810 nm. For our analysis, wavelengths of 520 nm, 560 nm, and 610 nm were selected for NO$_3^-$, NO$_2^-$, and NH$_4^+$ concentration, respectively., with detection limits of 0.1–50.0 mg L^{-1} for NO$_3^-$, 0.02–1.0 mg L^{-1} for NO$_2^-$, and 0.01–5.00 mg L^{-1} for NH$_4^+$. Following a standardized protocol, specific reagents were added to the samples, allowing the reactions to develop colour and the concentrations were then measured photometrically.

2.45. Inorganic nitrogen ~~Isotope~~isotope analyses

To trace microbial N transformations processes in the groundwater samples, inorganic N isotope analyses were performed with specific bacterial strains *Pseudomonas aureofaciens* for NO$_3^-$ and *Stenotrophomonas nitritireducens* for NO$_2^-$ isotopes. These strains carry out denitrification with N$_2$O as the end product, as they lack the N$_2$O reductase gene (Böhlke et al., 2007; Sigman et al., 2001). The detailed laboratory protocol encompassing the preparation and handling of the bacterial species, along with sample addition and isotope analysis is ~~mentioned~~available in previous publication (Deb and Lewicka-Szczebak, 2024). Gas samples were transferred from the headspace to previously evacuated Exetainer vials (Labco Limited, Ceredigion, UK), diluted and analyzed for isotope values δ^{15}N and δ^{18}O values of N$_2$O using mass spectrometry (Thermo Scientific, MAT 253 Plus mass spectrometer combined with GasBench and Precon) in the Laboratory of Isotope Geology and Geoecology at the University of Wrocław, Poland.

~~**2.5. Laboratory Incubation of Groundwater Samples**~~

~~Laboratory incubation studies were conducted with groundwater samples from 4 selected piezometers (P, abbreviated for piezometer: P-7, P-16, P-20, and P-23) with high nitrate concentrations to investigate natural nitrate reduction and identify favorable conditions for denitrification. A volume of 150 mL of groundwater from each piezometer was transferred into sterile 250 mL flasks, with each sample prepared in four replicates along with sterile controls. Sterile samples were produced by filtering the groundwater through 0.45 μm filters followed by the addition of 2 mL of HgCl$_2$ to inhibit microbial activity. These sterile samples served as controls for comparison with active treatments. The incubation flasks with groundwater samples were flushed with N$_2$ gas for 15 minutes, with the flow rate 60–70 mL min^{-1} and 0.6 Bar, to create suboxic conditions of similar O$_2$ content as in the studied aquifer. The final O$_2$ concentration in the headspace was about 5%, which corresponds to the dissolved O$_2$ content in water of 2.1 mg L^{-1} (Table 2). The pH of the samples, approximately 6.5 for each, was maintained without any adjustments. Prior to incubation, a low amount of ^{15}N-NO$_3^-$ labelled tracer was added to each sample based on its initial nitrate concentration resulting in at% ^{15}N (Atom Percent ^{15}N) of 0.4296%–0.4700%, slightly exceeding the natural abundance (0.366%), to trace N transformation pathways. The target δ^{15}N value of final NO$_3^-$ was 200‰. A stock solution was prepared by dissolving 12.1429 mg of Na^{15}NO$_3$ (99% ^{15}N) in 50 mL of water. From this, 1 mL was added to samples P-7, P-16, and P-20, while 2 mL was added to P-23. 1 mL of glucose, equivalent to the addition of 616 mg of C, was added as an additional carbon source after one week of incubation to stimulate microbial activity and enhance denitrification. All samples were incubated in dark for three weeks at 16 °C with agitation at 90 rpm.~~

304 The denitrifier method using *Pseudomonas aureofaciens* enabled isotope analysis of NO_3^- at
305 concentrations as low as 40 nmol NO_3^- L^{-1} (Stock et al., 2021, Deb and Lewicka-Szczebak 2024),
306 while using *Stenotrophomonas nitritireducens* allowed for NO_2^- analysis at concentrations as low
307 as 150 nmol NO_2^- L^{-1} (Deb and Lewicka-Szczebak, 2025).
308 The isotope analyses of NH_4^+ could not be performed due to mostly very low NH_4^+ concentrations,
309 below the detection limit of the isotope NH_4^+ analysis.
310
311 ## 2.6 Gas
312 Table 2: Data on GC headspace gas analyses for O_2, CO_2 and N_2O.
313 The average values and standards deviations of 4 repeated incubation flasks are shown. The
314 respective: dissolved O_2 concentration, N_2O production and CO_2 production were calculated
315 taking into account the gas constant for gases dissolution in water for the incubation temperature
316 of 16 C. For sterile samples the average data for the samplings before glucose addition (1 and 3)
317 and after glucose addition (4+6).
318

piezometer	sampling	day	O_2 [%] average	stdev	Dissolved O_2 [mg L^{-1}]	CO_2 [ppm] average	stdev	N_2O [ppb] average	stdev	N_2O production µg/L/d	CO_2 production mg/L/d
P7	1	2	8.5	1.5	3.5	865	225	918	189	0.66	1.82
P16	1	2	7.6	1.2	3.2	761	184	524	311	0.38	1.60
P20	1	2	7.3	1.6	3.0	391	48	258	179	0.18	0.82
P23	1	2	7.9	0.7	3.3	575	50	365	178	0.26	1.21
P7	3	7	4.3	2.3	1.8	1755	145	3316	3378	0.82	2.88
P16	3	7	3.2	1.4	1.3	1129	234	540	561	0.13	1.85
P20	3	7	3.8	1.4	1.6	337	156	527	547	0.13	0.55
P23	3	7	4.4	1.2	1.8	762	129	654	257	0.16	1.25
flushing + glucose addition											
P7	4	9	4.2	1.5	1.7	1340	294	393	246	0.28	2.82
P16	4	9	4.4	1.3	1.8	781	329	1290	1157	0.92	1.65
P20	4	9	2.6	1.1	1.1	426	399	133	85	0.10	0.90
P23	4	9	2.4	0.9	1.0	326	283	497	374	0.36	0.69
P7	6	14	3.9	2.2	1.6	1195	1545	5993	5657	1.49	1.96
P16	6	14	2.9	1.4	1.2	1823	1369	46578	91114	11.58	2.99
P20	6	14	2.4	1.2	1.0	1908	475	4459	7284	1.11	3.13
P23	6	14	4.1	2.0	1.7	1807	774	2052	2050	0.51	2.96
Sterile samples											
P7	1+3	4	4.4		3.0	1928		70		0.03	3.43
P16	1+3	4	8.1		4.0	2160		224		0.09	3.84
P20	1+3	4	5.5		2.6	632		0		0.00	1.12
P23	1+3	4	6.4		3.3	1205		0		0.00	2.14

							flushing + glucose addition
P7	4+6	4	3.5	2.6	1381	218	0.08	2.46
P16	4+6	4	3.5	1.7	1299	1654	0.64	2.31
P20	4+6	4	2.3	1.1	387	106	0.04	0.69
P23	4+6	4	2.6	0.8	1044	517	0.20	1.86

Headspace samples were periodically collected to measure N_2O, CO_2 and O_2 concentration and N_2O isotope signatures, providing insights into nitrate reduction and denitrification processes under anoxiccontrolled sub-oxic conditions. The samples of 25 mL of headspace gas were collected each second day into pre-evacuated 12 mL Labco Exetainers (1 Bar overpressure). The sampled gas volume was replaced with pure N_2 gas. The headspace samples were analysed on the gas chromatograph Shimadzu GC Nexis 2030 equipped with barrier discharge ionisation detector (BID) and thermal conductivity detector (TCD) for O_2, CO_2 and N_2O concentration (Bucha et al., 2025). The N_2O gas was analysed for $\delta^{15}N$, $\delta^{18}O$ and $\delta^{15}N^{SP}$ (difference between $\delta^{15}N$ values between central and terminal position of N in the linear N_2O molecule) using cavity ring-down spectroscopy (CRDS) by Picarro G5131-i spectrometer equipped with small sample injection module (SSIM) and connected to SRI autosampler (Eckhardt et al., unpublished) in Laboratory of Isotope Geology and Geoecology at the University of Wrocław. The isotope analytical limit was about 300 ppb N_2O, for this ambient concentration the measurement precision was better than 0.5‰ for $\delta^{15}N$ and $\delta^{18}O$ and better than 1‰ for $\delta^{15}N^{SP}$. Since this is a newly developed measurement technique, the controlled measurements for selected sampling points were performed at Thünen Institute, Braunschweig, Germany applying mass spectrometry (MS) (Thermo Scientific, 5 collector Delta V mass spectrometer combined with Trace GC and Precon) (Lewicka-Szczebak et al., 2020). After applying proper corrections to CRDS technique (Harris et al., 2020) and isotope normalization with the same sets of standards (two isotope standards for normalization: DASIM 16 and 17 (Well et al., 2025) and at least three standards of different N_2O concentration) the results between both approaches showed good repeatability within up to 2‰ difference for $\delta^{15}N$ and $\delta^{18}O$ and up to 4‰ difference for $\delta^{15}N^{SP}$, which fits withing typical reasonable range for comparing measurements with different techniques (Mohn et al., 2014). For sterile samples (with $HgCl_2$ addition) the CRDS technique gave erogenous results, thus only MS results were accepted. The N_2O isotope results were evaluated using modeling software FRAME (isotope FRactionation And Mixing Evaluation) (https://malewick.github.io/frame/) to identify N_2O production pathways and quantify N_2O reduction to N_2 (Lewicki et al., 2022).

Inorganic N levels in incubated samples were analyzed at the beginning, after one week of incubation before glucose addition, and at the end of the experiment. Additionally, the isotopic signatures of inorganic N were determined using bacterial denitrification by *Pseudomonas aureofaciens* and *Stenotrophomonas nitritireducens*. The N_2O gas formed during this conversion, representing nitrate or nitrite isotope signatures $\delta^{15}N$ and $\delta^{18}O$, was measured with mass spectrometry (Thermo Scientific, MAT 253 Plus mass spectrometer combined with GasBench and Precon).

2.67. DNA extraction and qPCR analyses for the field and experimental samples
For DNA extraction, the groundwater samples were filtered using sterile 0.45 μm mixed cellulose esters (MCE-) membrane filters. The filters were stored at −80 °C for subsequent analysis. DNA was extracted from 250 mg of water filters using the DNeasy® PowerSoil® Pro Kit (Qiagen,

359 Germany), following the manufacturer's protocol with a modification: samples were homogenized
360 using a Precellys 24 homogenizer (Bertin Technologies, France) at 5000 rpm for 20 seconds. DNA
361 concentration and quality were assessed using a TECAN Infinite M200 spectrophotometer, and
362 the extracted DNA was stored at −20 °C for further microbial analysis.
363 qPCR (quantitative Polymerase Chain Reaction) was used to quantify the bacterial and archaeal
364 16S rRNA genes, as well as the abundances of genes involved in denitrification (*nirS, nirK, nosZI,*
365 *and nosZII),* nitrification (bacterial, archaeal, and comammox (complete ammonia oxidation),
366 *amoA*), nitrogen fixation *(nifH) and* dissimilatory nitrate reduction to ammonium (DNRA, *nrfA*).
367 qPCR reactions were performed using a Rotor-Gene Q thermocycler (Qiagen, Germany). The 10
368 µl reaction mixture consisted of 1 µl of extracted DNA, forward and reverse gene-specific primers,
369 5 µl of Maxima SYBR Green Master mix reagent (Thermo Fisher Scientific, Waltham, MA, USA),
370 and MilliQ water. Each sample was amplified in duplicate, with DNA-free negative control
371 samples included in every run. The thermal cycling conditions and primers used are detailed in
372 Table.3S3 (Espenberg et al., 2024). qPCR results were analyzed using Rotor-Gene® Q software
373 v.2.0.2 (Qiagen) and LinRegPCR v.2020.2 (Netherlands). The number of gene copies was
374 calculated based on standard curve ranges (Espenberg et al., 2018; Kuusemets et al., 2024) and
375 expressed as gene copies per ml of water (copies mL^{-1}). DNA extraction and qPCR analysis were
376 conducted in the Department of Geography at the University of Tartu, Estonia.
377
378
379
380 Table 3: qPCR primer pairs and programs for targeted genes

Target gene	Primer	Primer concentration (µM)	Program	
bacterial 16S rRNA	Bact517F	0.3	95°C 30s; 60°C 45s; 72°C 45s	x 40 cycles
	Bact1028R			
archaeal 16S rRNA	Arc519F	0.3	95°C 15 s;56°C 30 s; 72°C 30 s	x 45 cycles
	Arch910R			
nirK	nirK876	0.4	95°C 15 s, 58°C 30 s; 72°C 30s, 80°C 30 s	x 45 cycles
	nirK1040			
nirS	nirSCd3af	0.4	95°C 15 s, 55°C 30 s; 72°C 30s, 80°C 30 s	x 45 cycles
	nirSR3cd			
nosZI	nosZ2F	0.4	95°C 15 s, 60°C 30 s, 72°C 30 s, 80°C 30s	x 45 cycles
	nosZ2R			
nosZII	nosZIIF	1	95°C 30 s, 54°C 45 s, 72°C 45 s, 80°C 45 s	x 45 cycles
	nosZIIR			
bacterial amoA	amoA-1F	0.4	95°C 30 s, 57°C 45 s, 72°C 45 s	x 45 cycles
	amoA-2R			
archaeal amoA	CrenamoA 23F	0.4	95°C 30 s, 55°C 45 s, 72°C 45 s	x 45 cycles
	CrenamoA 616R			
comammox amoA	comamoA AF	0.6	95 °C 15 s, 55 °C 30 s, 72 °C 30 s	x 40 cycles
	comamoA SR			
nrfA	nrfAF2awMOD	0.6	95 °C 15 s, 56 °C 30 s, 72 °C 30 s	x 45 cycles
	nrfAR1MOD			
nifHA	Ueda19F	0.4	95 °C 30 s, 53 °C 45 s, 72 °C 45 s	x 45 cycles
	Ueda407R			

3. Results

3.1. Dissolved inorganic N compounds

3.1.1. Inorganic nitrogen (NO$_3^-$, NO$_2^-$, NH$_4^+$) content and isotope signatures of initial field groundwater samples

Initial field samples were measured for inorganic N to determine NO$_3^-$, NO$_2^-$, and NH$_4^+$ concentration and identify piezometers with the highest nitrate levels, which were then selected for laboratory incubation studies. While field measurements provided baseline reference concentrations of NO$_3^-$, NO$_2^-$, and NH$_4^+$, the laboratory incubation samples revealed significant changes in these concentrations over the incubation period, highlighting N transformation processes under controlled conditions.

Initial field samples before the start of incubation showed NO$_3^-$ concentration from 0.2 mg N L^{-1} to 89.5 mg N L^{-1}, NO$_2^-$ concentration from 0.02 to 0.4 mg N L^{-1} and NH$_4^+$ ~~-~~concentration from 0.02 to 17.95 mg N L^{-1} (Table ~~1~~S1). The four samples with especially high nitrate concentration level ranging from 32.8 to 89.9 mg N L^{-1} have been selected for further incubation studies (Table ~~1).~~S1). These samples showed very low NH$_4^+$ concentration. Only a few piezometers showed higher NH$_4^+$ contents, which was associated with low NO$_3^-$ levels, rather low DON and high DOC (Table S1).

NO$_3^-$ concentration was determined in 23 samples and NO$_2^-$ in 22, with one sample below the detection limit for NO$_2^-$ (Table ~~1~~S1). But out of these 23 samples, isotope analysis of δ^{15}~~N-NO$_3$~~N$_{NO3-}$ and δ^{18}O$_{NO3}$ ~~was successful~~ could have been performed on 12 samples, while δ^{15}N$_{NO2}$ and δ^{18}O$_{NO2}$ could be analyzed for 7 samples only (Table ~~1), with the remainder samples below the~~S1), due to detection limit of the applied methods for isotopic analysis. NH$_4^+$ isotopic signature was not determined because of very low concentrations mostly below detection limit for the isotope analysis. All the isotope results are presented in the following figures in the frame of literature data for typical nitrate sources and denitrifying processes (Fig. 3A) and typical ammonium sources and nitrifying N transformation processes (Fig. 3B) after (Deb et al., 2024). Such visual presentation is applied for better identification of possible N sources and N transformations.

416
417

418
419
420
421
422
423
424
425

14
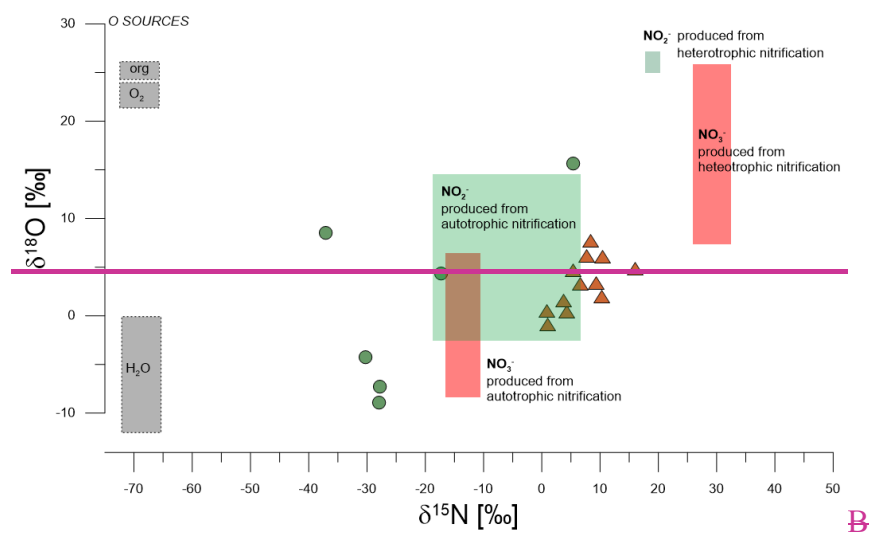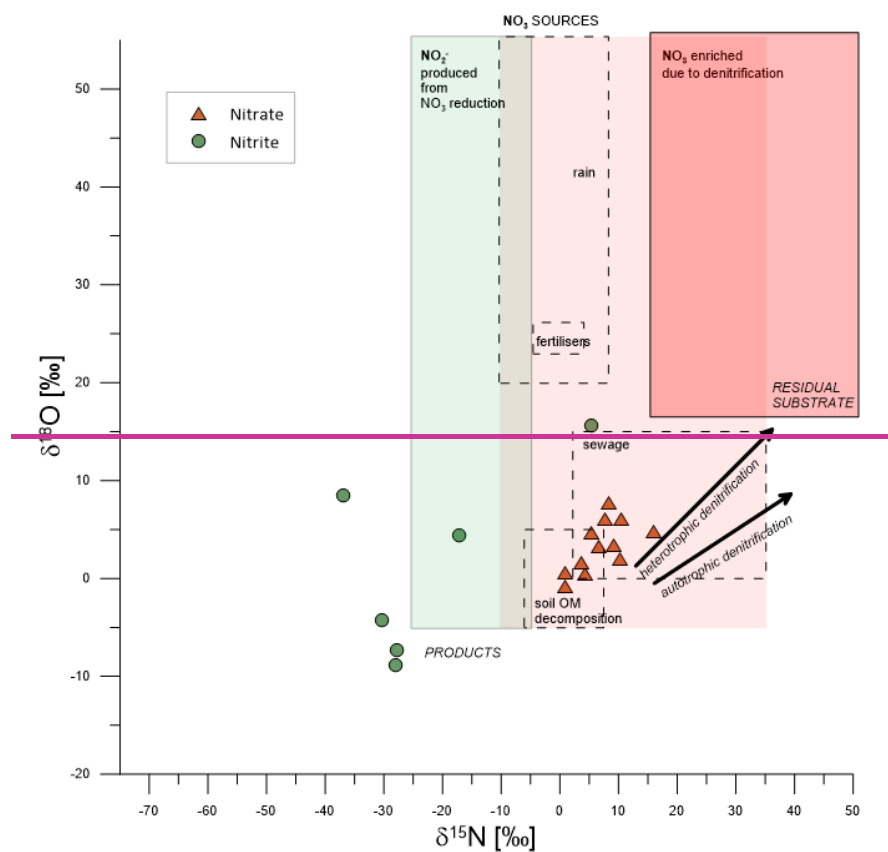
Figure 3: The isotope signatures of NO₃⁻ (orange triangles) and NO₂⁻ (~~green~~blue circles) in field groundwater samples presented with the literature data for particular N sources and isotope effects for main N transformations, with respect to denitrification processes (A) and nitrification nitrite and nitrate sources (B). The literature data shown as boxes after ~~-~~(Deb et al., 2024). In (A) NO₃⁻ sources (light pink rectangles) include rain, fertilizers, sewage, and soil organic matter, while products (light green rectangle) include NO₂⁻, formed during NO₃⁻ reduction. Residual NO₃⁻ enriched through denitrification is represented in the red rectangle. Arrows depict typical isotope ~~effect~~effects associated with autotrophic and heterotrophic processes. In (B) isotopic characteristics of NO₂⁻ (blue~~-~~green rectangles) and NO₃⁻ (~~red~~light orange rectangles) originating from autotrophic and heterotrophic nitrification is shown. Grey rectangles illustrate possible oxygen sources (O₂ and H₂O) used during nitrifying oxidation processes.

In Fig. 3A the light pink-shaded zone reflects NO₃⁻ contributions from different sources such as fertilizers, sewage, and soil organic matter decomposition, with minimal microbial transformation. The red-shaded 'Residual Substrate' zone, indicates the product of advanced denitrification, i.e. residual nitrate enriched in ^{15}N and ^{18}O due to preferential reduction of light isotopes. The correlation between δ^{18}O and δ^{15}N values of nitrate is typical for isotope enrichment due to heterotrophic denitrification leading to ^{18}O and ^{15}N enriched of the residual NO₃⁻. The light green-shaded area represents NO₂⁻ produced from NO₃⁻ reduction during partial denitrification, an intermediate step in denitrification. The isotopic patterns also differentiate between autotrophic and heterotrophic denitrification. Samples aligning with autotrophic denitrification indicate the reduction of NO₃⁻ coupled with the oxidation of inorganic compounds like sulfur or hydrogen, resulting in a slower rate of isotopic fractionation and less pronounced enrichment in δ^{15}N and δ^{18}O (Cui et al., 2019; Hu et al., 2024). In contrast, samples reflecting heterotrophic denitrification show rapid isotopic fractionation due to the use of organic carbon as the electron donor, leading to greater enrichment of δ^{15}N and δ^{18}O in the residual nitrate (Deb et al., 2024).
This study NO₃⁻ samples (orange triangles, Fig. 3A) are located in the area typical for NO₃⁻ originating from organic matter decomposition and of sewage origin. This study NO₂⁻ samples (blue circles, Fig. 3A), are mostly shifted towards lower δ^{15}N values, with the expected isotope effect typical for denitrification NO₃⁻ reduction to NO₂⁻, with isotopically depleted NO₂⁻ due to the preferential reduction of light isotopes (^{14}N and ^{16}O). $\delta^{18}O_{NO2}$ values are similar or lower than the respective NO₃⁻ source, which may indicate additional incorporation of water into the formed NO₂⁻.
Figure 3B illustrates the isotopic composition of nitrate (NO₃⁻) and nitrite (NO₂⁻) in groundwater samples in regard to possible nitrification processes. Autotrophic nitrification, with NO₃⁻ produced from NH₄⁺ or organic nitrogen, is characterized by lower δ^{15}N and δ^{18}O values, while heterotrophic nitrification contributes to NO₃⁻ and NO₂⁻ production with distinct isotopic enrichment from organic nitrogen compounds.
This study NO₃⁻samples (orange triangles, Fig. 3B) are located between values typical for NO₃⁻ production from autotrophic and heterotrophic nitrification, the observed correlation might be a mixing between these two NO₃⁻ origins. However, from the NO₂⁻ samples (blue circles, Fig. 3B) only two points indicate typical values for autotrophic nitrification, whereas others show much lower δ^{15}N values.

3.1.2 Inorganic nitrogen (NO_3^-, NO_2^-, NH_4^+) content and isotope signatures during incubation

During the first phase (before glucose addition), NO_3^- concentrations decreased significantly across all samples (decrease of 14 to 33 mg L^{-1} N was noted, Fig.4A). Concurrently, NO_2^- concentrations increased significantly reaching around 3.7 to 13.5 mg L^{-1} N, (Fig.4A). In the second phase (after glucose addition), NO_3^- concentrations continue to decrease in all samples (further decrease of 6.2 to 47.6 mg L^{-1} N compared to day 7 sample, Fig.4A), while NO_2^- levels further increase for most samples reaching 4.7 to 13.5 mg L^{-1} N. NH_4^+ concentrations were very low from 0 to 0.2 mg L^{-1} N) and remained largely unchanged throughout the incubation period.

Further, the isotopic signatures of nitrate ($\delta^{15}N_{NO_3}$ and $\delta^{18}O_{NO_3}$) and nitrite ($\delta^{15}N_{NO_2}$ and $\delta^{18}O_{NO_2}$) were analysed in water samples during laboratory incubation (Fig 4B). $\delta^{15}N_{NO_3}$ shows much higher values when compared to initial field samples (Fig. 3) due to low addition of ^{15}N-NO_3^- tracer. The preparation of tracer solution and amount of tracer addition was calculated to attain ca. 100-200 ‰ as the final $\delta^{15}N_{NO3}$ value. However, due to different initial NO_3^- concentrations and precision of the low amount tracer addition, our final $\delta^{15}N_{NO3}$ after tracer addition is variable for each of the four incubated samples from approximately 100‰ for P-23 to over 300‰ for P-20 (Fig. 4B). However, these different final values have been taken into account by all calculations and modelling, so that the differences did not impact the data interpretation. All calculations were applied individually for each incubated water sample and individual $\delta^{15}N_{NO3}$ values have been accepted as the incubation starting point for each of the four water samples.

$\delta^{15}N_{NO_3}$ and $\delta^{18}O_{NO_3}$ increase significantly during the first phase of incubation and remain quite stable during the second incubation phase across all samples. $\delta^{15}N_{NO_2}$ shows slight variability across all samples, with values ranging from approximately -50‰ to 0‰, hence much lower than the respective $\delta^{15}N_{NO_3}$ values. $\delta^{18}O_{NO_2}$ shows very dynamic variations without very consistent trends, reflecting the complexity of microbial and environmental interactions affecting nitrite transformation. Interestingly, there is very clear pattern for P-7, P-16 and P-20 with significant $\delta^{18}O_{NO_2}$ enrichment for the 2nd sampling (7 days) and further depletion for the 3rd sampling (14 days) (Fig. 4B).

In the sterile treatment the NO_3^- reduction is even faster than in other samples, while the isotope signatures are very stable showing very minoronly negligible isotope enrichment. NO_2^- concentrations are verystay low not exceeding 0.3 mg N L^{-1}. NH_4^+ concentrations increase during the incubation reaching up to 4 mg N L^{-1}, which is much higher than observed for non-sterile samples.

A. Inorganic N content	B. Inorganic N isotope signatures
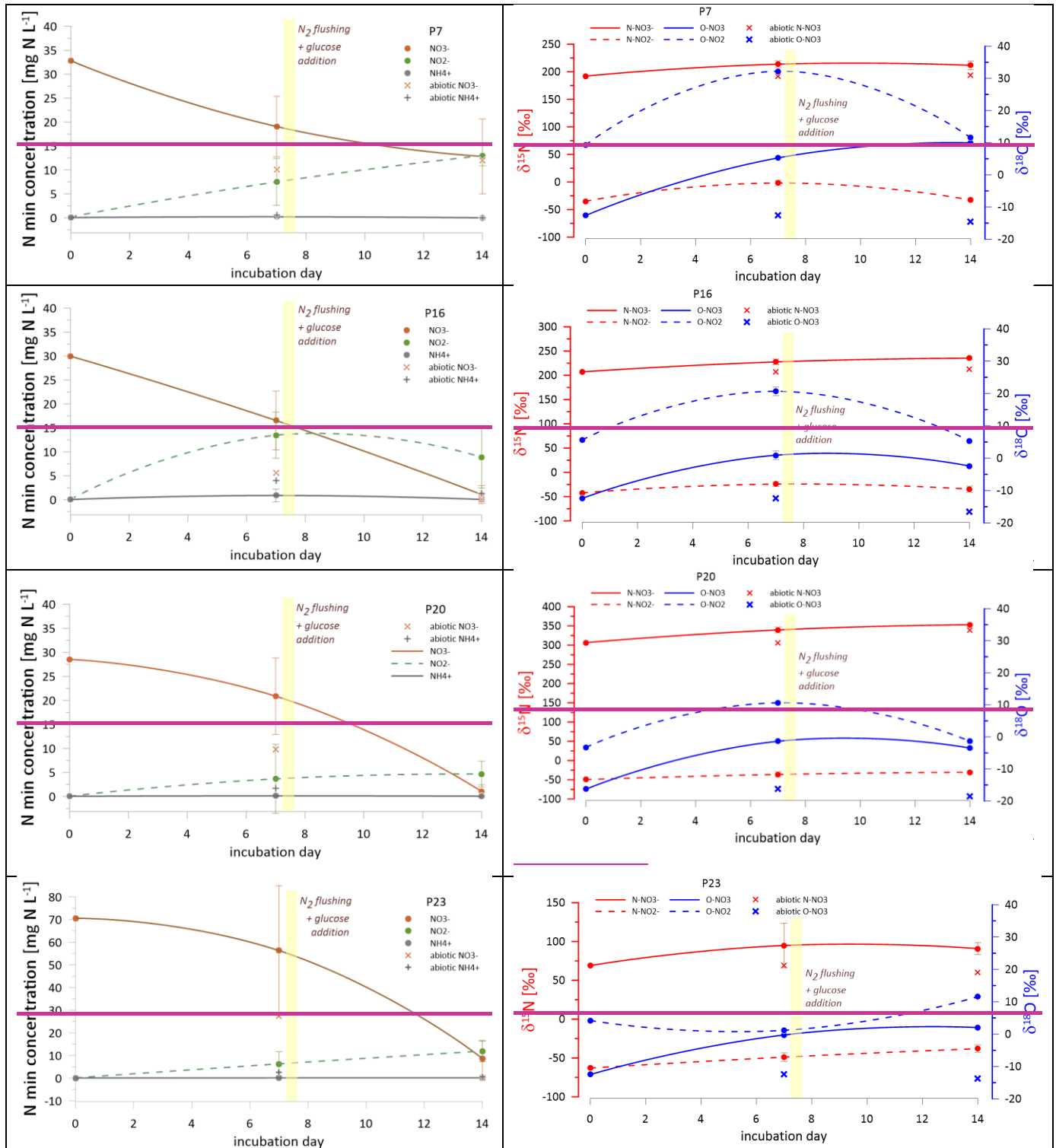
510 **Figure: 4. Content of inorganic nitrogen forms (orange line: NO₃⁻, green line: NO₂⁻, grey**
511 **line: NH₄⁺) (A) and their isotopic signatures (δ¹⁵N and δ¹⁸O) (B) during laboratory**

incubation. The graphs in A show concentrations variation in time and graphs in B depict changes in δ¹⁵N (dark red lines) and δ¹⁸O (blue lines) values over time for ~~nitrate~~NO₃⁻ (solid line) and ~~nitrite~~NO₂⁻ (dashed line) in different samples (P, abbreviated for piezometer: P-7, P-16, P-20, and P-23), illustrating dynamic isotopic variations influenced by microbial processes. Sterile samples are shown as the individual points on the graphs (for NO₃⁻ and NH₄⁺ contents, while NO₂⁻ was very low for all the sterile samples, and is not shown).

3.1.3 Isotope mass balance and source attribution for incubation study

To quantify the NO_2^- sources during incubation experiment, a simple isotope mass balance approach was applied based on $\delta^{15}N$ measurements of NO_3^- and NO_2^-. Based on the observed $\delta^{15}N_{NO3\ 0}$ (initial value, day 0) and change in $\delta^{15}N_{NO_2}$ values (between day 0 and day 7 of the incubation) we can calculate the maximal contribution of NO_2^- originating from NO_3^- reduction (NAR) in this new-formed NO_2^- applying the isotope mass balance (Eq.1). These calculations are simplified by neglecting any isotope fractionation of the NO_2^- pool.

$$NAR = \frac{\delta^{15}N_{NO2-7} - \delta^{15}N_{NO2-0}}{\delta^{15}N_{NO3-0}} \qquad\qquad (Eq.1)$$

Table 1: Inputs and results of the mass balance calculations for determining the contribution of nitrate reduction (NAR) in the nitrite pool with Eq.1: $\Delta\delta^{15}N_{NO_2}$ is the change of nitrite N isotope signature between day 0 and day 7, $\delta^{15}N_{NO3-0}$ – initial N isotope signature of nitrate, $\Delta[NO_2^-]$ is the change of nitrite concentration between day 0 and day 7, NAR is the amount of produced nitrite originating from NAR, $\Delta[NO_3^-]$ is the nitrate consumption between day 0 and day 7.

The calculation results (Table 1) indicate that from 0.2 up to 1.3 mg N-NO_2^- L^{-1} originates from NAR, which is low amount when compared to the magnitude of N-NO_3^- consumption of 13.7 to 33.2 mg L^{-1} (Table 1). But interestingly, the large majority of N-NO_2^- (80 to 95 %) originates from other transformations than NO_3^- reduction.

A closer look on the isotopic analysis of nitrite (NO_2^-) in the groundwater incubation study (Fig. 5) reveals that the highest nitrite concentrations are characterised by the lowest isotope signatures. We observe a statistically significant correlation between O and N isotopic signatures of NO_2^-. Theoretically, this could be the mixing line with the ^{15}N labelled values originating from labelled NO_3^- reduction, but this NO_3^-, shows low $\delta^{18}O$ values in the range from -16 to +10‰. Hence, this rather shows mixing of the different origins of unlabelled NO_2, which is in great majority (as shown above and in Table 1), potentially originating from both autotrophic and heterotrophic nitrification processes.

556
557
558
559 **Figure 5: Isotopic Signatures of Nitrite (NO_2^-) during laboratory Incubation: first phase,**
560 **before glucose addition: empty circles, second phase, after glucose addition: filled circles.**
561 The points size is proportional to nitrite concentration. The shaded regions correspond to isotopic
562 ranges associated with autotrophic and heterotrophic nitrification (after (Deb et al., 2024)),
563 illustrating a shift in processes following glucose addition.
564
565 **3.2. Gas headspace sample analysis and FRAME modelling**
566 For almost all samplings significant N_2O and CO_2 fluxes were observed during the incubation. The
567 gases were accumulated in the headspace until day 7 of the incubation (phase 1: day 1 – day 7),
568 then after flushing the accumulation was started again for next 7 days (phase 2: day 8 – day 14).
569 Table 2S2 shows results of headspace gas analyses for the second and last day of the accumulation,
570 for each incubation phase, before and after glucose addition. The CO_2 production varies from 0.7
571 to 3.1 mg L^{-1} day^{-1} with similar flux range for both phases. The N_2O production varies from 0.1 to
572 11.6 μg L^{-1} day^{-1} with significantly higher fluxes for the second incubation phase, with one
573 extremely high outlier.
574 Sterile samples show CO_2 production in the comparable amount to unsterile treatments, and much
575 lower N_2O production, however still significant for some points, especially for the second
576 incubation phase after glucose addition (Table 2S2).
577 Figure 56 shows the isotopic signatures ($\delta^{15}N^{SP}$, $\delta^{18}O$, $\delta^{15}N$) of N_2O in headspace samples from
578 laboratory incubation before and after glucose addition together with the main N_2O production
579 pathways and typical N_2O reduction line summarized after literature data (Yu et al., 2020). The
580 isotope characteristics for the main N_2O production pathways: bacterial and fungal denitrification
581 (bD and fD), nitrifier denitrification (nD), nitrification (Ni) and chemodenitrification (chD) are
582 shown for the particular substrate isotopic signatures of the actual case study: $\delta^{18}O_{H2O}$ of -9.0‰
583 (mean common value for all water samples) and respective $\delta^{15}N_{NO3}$, separately determined for
584 each sampling point (respective values in Table 1S1).
585
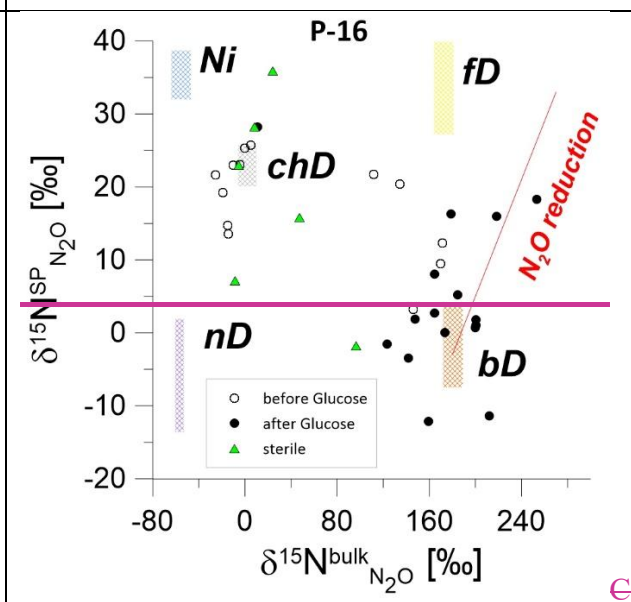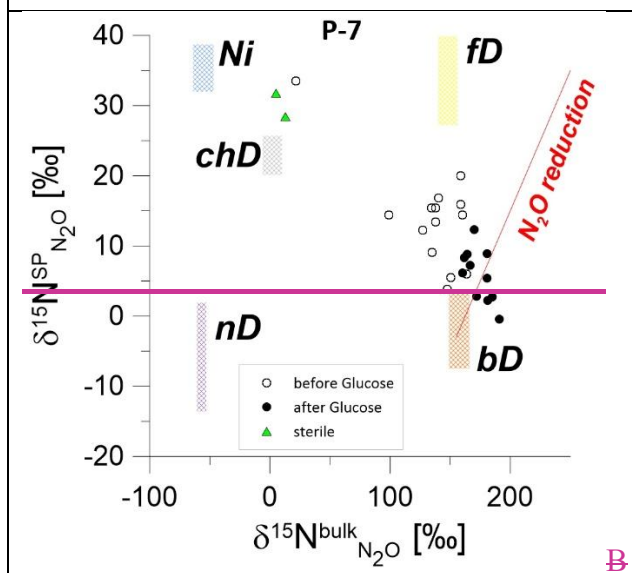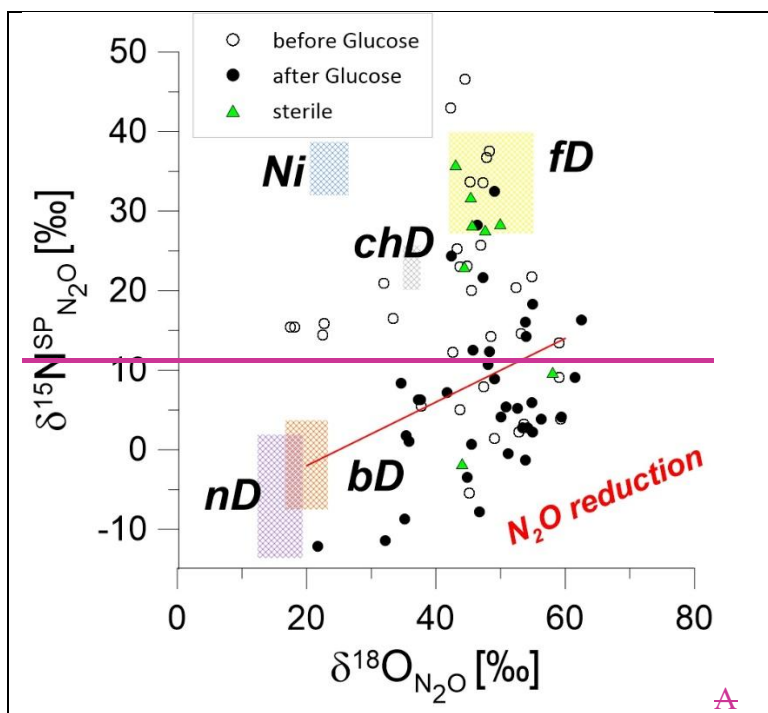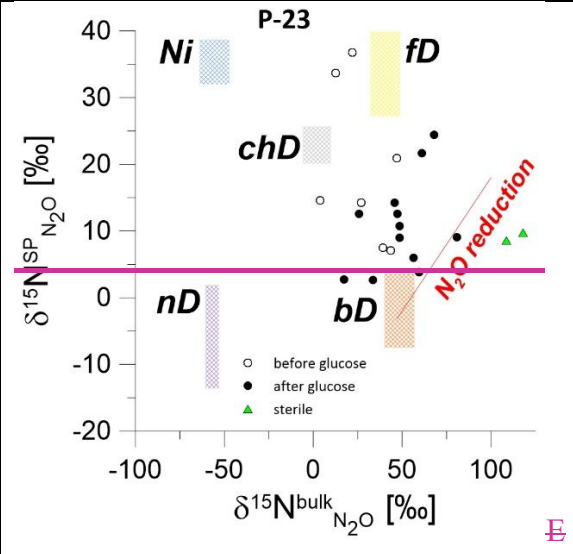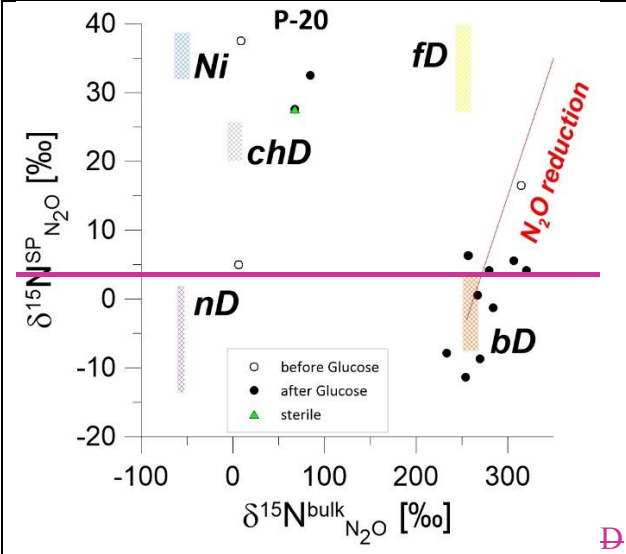
587
588
589
590
591 **Figure ~~5~~ 6: Isotopic signatures ($\delta^{15}N^{SP}_{N2O}$, $\delta^{18}O_{N2O}$ and $\delta^{15}N_{N2O}$) highlighting N₂O dynamics**
592 **and microbial nitrogen transformation pathways during laboratory incubation for**
593 **groundwater samples (P, abbreviated for piezometer: P-7, P-16, P-20, and P-23). Empty**
594 **circles represent the first incubation phase, filled circles – the second incubation phase after**
595 **glucose addition and green triangles show sterile samples. Clustering reflects a shift from**
596 **mixed nitrification and denitrification before glucose addition to bacterial denitrification**
597 **dominance after glucose addition. Panel A presents $\delta^{15}N^{SP}$-$\delta^{18}O$ map for all samples, since**
598 **the source processes are common for all samples, panels B-E present $\delta^{15}N^{SP}$-$\delta^{15}N$ maps**
599 **individually plotted for each piezometers, because depending on the particular ^{15}N content**
600 **for each piezometer the mixing endmembers isotopic signatures (bD and fD) differ. Each**
601 **plot shows isotopic values before glucose addition (white circles) and after glucose addition**
602 **(black circles), reflecting microbial processes like bacterial denitrification (bD), autotrophic**
603 **nitrification (Ni), nitrifier denitrification (nD), and fungal denitrification (fD), with N₂O**
604 **reduction along the red line.**
605
606 Before glucose addition the isotopic signatures indicate mixing between nitrification and
607 denitrification processes (Fig. 6A). In P-7, before glucose addition, isotopic data clustered near the
608 nitrifier denitrification (nD) zone, highlighting ammonia oxidation and partial N₂O reduction (Fig.
609 6B). In P-16, isotope signatures are widely distributed between nitrifier and bacterial
610 denitrification zones, suggesting overlapping processes (Fig. 6C). In P-20 and P-23, clustering
611 near the bacterial denitrification (bD) zone reflected nitrate reduction as the dominant pathway
612 with minimal N₂O reduction (Fig. 6D,6E).
613 After glucose addition, the isotopic data indicate that N₂O production was primarily driven by
614 bacterial denitrification (bD), with relatively low $\delta^{15}N^{SP}_{N2O}$ and $\delta^{18}O_{N2O}$ values, clustering mostly
615 around reduction line (Fig. 6A). In the $\delta^{15}N^{SP}$- $\delta^{15}N$ space, mostly the isotopic data showed a clear
616 shift toward bD, supported by a significant increase in $\delta^{15}N_{N2O}$ values, indicating N₂O production
617 from the slightly ^{15}N-labeled NO_3^- pool and some effect of N₂O reduction (Fig. 6B-E). In P-23,
618 however, the data indicate more possible pathways mixture, including nitrification (Ni) and fungal
619 denitrification (fD) (Fig. 6E). Significant reduction of N₂O to N₂ can be supposed based on the
620 clustering of the points along the N₂O reduction line, especially in the $\delta^{15}N^{SP}$- $\delta^{18}O$ isotope map
621 (Fig. 6A). In $\delta^{15}N^{SP}$- $\delta^{15}N$ isotope map the effect of N₂O reduction is less visible, because the
622 artificially elevated $\delta^{15}N$ values result in very steep reduction line. Minimal clustering near the
623 fungal denitrification (fD) zone suggests limited fungal contributions to N₂O production. However,
624 the $\delta^{15}N^{SP}$- $\delta^{18}O$ map shows some samples near the fD zone (Fig. 6A), and the FRAME model
625 (Fig. S1) also supports this with minor yet detectable fungal involvement. The shift in $\delta^{15}N^{SP}_{N2O}$
626 values reflects the changing dynamics, with nitrification and nitrifier denitrification becoming less
627 prominent as bacterial denitrification intensified in course of incubation.

628
629 These isotope results of N_2O from the headspace samples were jointly analyzed using the three
630 dimensional FRAME (FRActionation and Mixing Evaluation) model (Lewicki et al., 2022) to
631 quantitatively interpret the isotopic signatures of N_2O, identifying microbial pathways driving N_2O
632 production and estimating N_2O reduction progress. This offers the most precise insight into N
633 transformations under controlled experimental conditions.
634
635
636
637
638
639
640
641 The FRAME model outputs (Fig. S1), reveal distinct microbial processes driving N_2O production
642 and reduction during laboratory incubation of groundwater samples from piezometers P-7, P-16,
643 P-20, and P-23, comparing the initial incubation phase (1–2 days) to the later phase (4–14 days),
644 including samples before and after glucose addition.
645 This division of samples was made after the observed isotopic signatures – the initial samples (day
646 2) showed no ^{15}N enrichment in the N_2O and later samples (day 7 – day 14) were characterised
647 with very significant ^{15}N enrichment. Initially, autotrophic nitrification (Ni) dominated across all
648 samples, contributing around 60–70% to N_2O production, while bacterial denitrification (bD) was
649 lower, ranging between 20–30%. In P-7 and P-16, minor contributions from nitrifier denitrification
650 (nD) (10–20%) and fungal denitrification (fD) (<10%) were observed, with similar trends in P-20
651 and P-23, where nD accounted for slightly higher fractions of N_2O production. Residual N_2O
652 fractions (r_{N2O}) across all piezometers ranged between 10–26%, reflecting high partial N_2O
653 reduction to N_2.
654 In the later incubation phase, microbial activity shifted significantly toward denitrification, with
655 bD becoming the dominant pathway (up to 80–85%), driven by the availability of carbon. P-7 and
656 P-16 exhibited a gradual rise in bD, reaching up to 73%, while residual Ni contributions declined
657 correspondingly. In P-20 and P-23, the transition was sharper, with bD dominance occurring more
658 abruptly. Residual N_2O fractions decreased across all samples as bD activity intensified.
659 Simultaneously, Ni contributions dropped below 10% in all samples, while nD and fD remained
660 minimal, contributing <15% to N_2O production. However, for the last sample (day 14 of the
661 incubation) for all the analysed groundwater samples, the model could not find any solution. This
662 might be due to accumulation of very different N_2O origins and progressing reduction of N_2O
663 mixture of all production pathways.
664 Figure S2 presents illustration of the model performance on an example of sample 6 (day 14) of
665 the P-16, while this is similar for all the piezometers. The modelling problem occurs due to too
666 high $\delta^{18}O$ measured values, while $\delta^{15}N$ and $\delta^{15}N^{SP}$ show values typical for bD, $\delta^{18}O$ is shifted to
667 much higher values, indicating large reduction, not confirmed with low $\delta^{15}N^{SP}$ values.
668
669

670
671
672
673
674
675

3.3 Gene abundance and proportion analyses

The gene abundance graph (Fig 6A7A) illustrates the quantification of key nitrogen cycle genes while the proportions of functional genes relative to total prokaryotic abundance are shown in Fig 6B7B for groundwater samples (P-7, P-16, P-20, and P-23) before and after incubation.

The gene abundance results indicate that post-incubation, especially with glucose addition, led to a shift of microbial communities from predominantly archaeal ammonia oxidizers toward bacterial denitrifiers. Pre-incubation data indicate a notable presence of archaeal *amoA* genes compared to bacterial *amoA,* suggesting active archaeal ammonia oxidation in the samples (Fig. 7A). While denitrification gene *nosZI*—show relatively high abundance in some samples (e.g., P-16 and P-23), the consistent presence of archaeal *amoA* and the lower abundance of other denitrification-related genes (*nirK, nirS,*), suggests nitrification processes were prominent prior to incubation. This is particularly evident in P-7 and P-20, where archaeal *amoA* surpasses denitrification genes, suggesting a stronger nitrification potential. Post-incubation, there was a significant increase in the abundance of denitrification genes like *nosZI,* particularly in samples P-7, P-16 and P-20, illustrating a shift from nitrification to denitrification under incubation conditions Fig. 7A.

The abundance of archaeal 16S rRNA genes decreased in samples P-7 and P-23, indicating a reduction in archaeal community, whereas the abundance of bacterial 16S rRNA increased significantly in P-16 and P-20, reflecting bacterial growth during incubation. Paired T-tests confirmed these observations, showing significant increases in the abundance of *nosZI* genes in P7 ($p<0.05$) and P16 ($p<0.05$) and shifts in the archaeal 16S rRNA abundance ($p<0.05$), but not in the abundances of *nirK* or *nosZII* genes ($p>0.05$), highlighting the variability in microbial

24

697 responses.

Gene Abundance in Samples - Original vs After Incubation
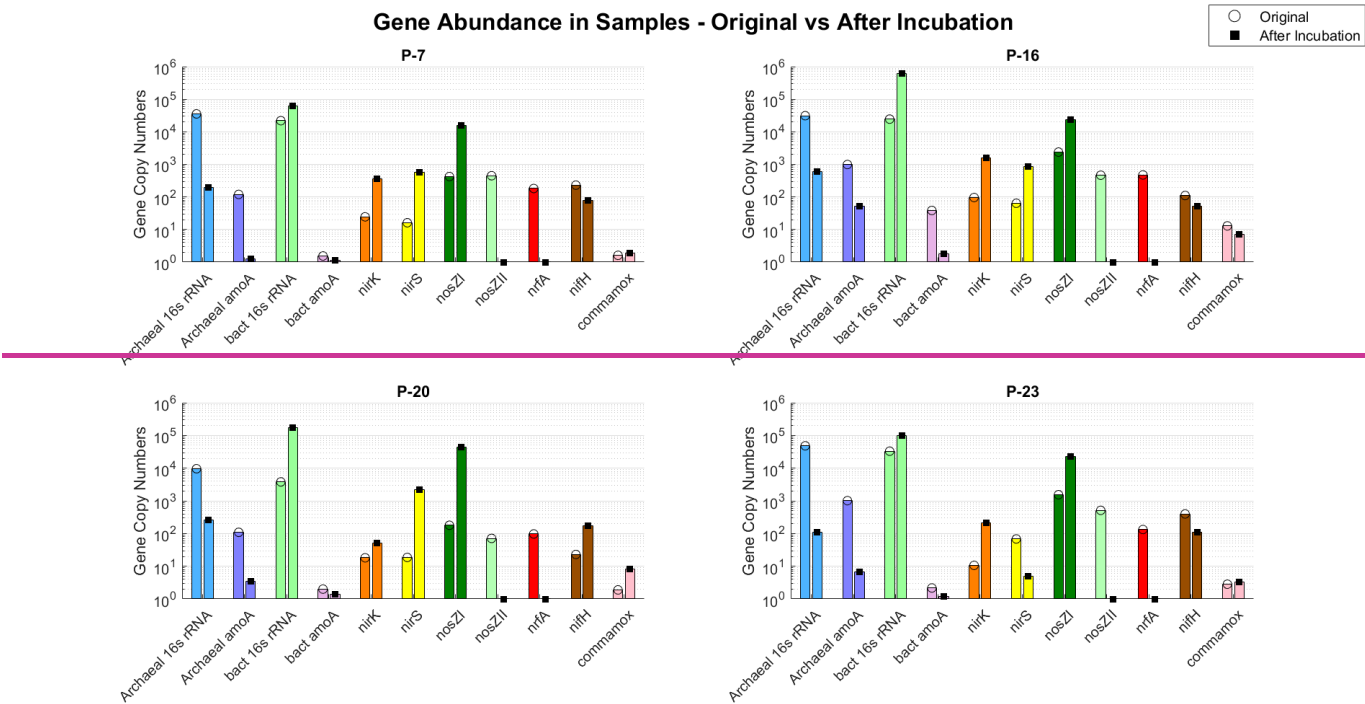
698
699
700
701
702
703
704
705
706
707
708
709
710
711
712
713
714 **Figure** 67: **Microbial Functional Gene Dynamics in Groundwater Samples (A**):) **Comparison**
715 **of gene abundance in groundwater samples** before and after incubation

716
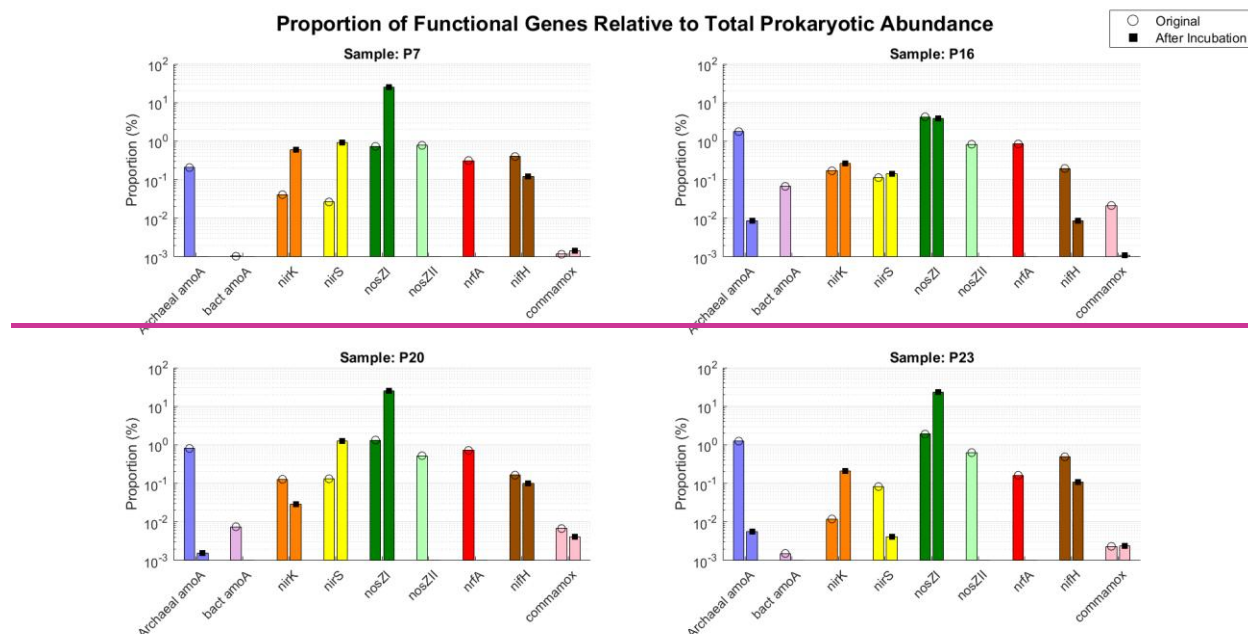
717 ~~Figure 6and~~ **(B)~~:~~) Functional Gene Proportions** ~~Pre-~~**in samples before** and ~~Post-~~

718 ~~Incubation~~ **after incubation**

719

720 The graphs (Fig. ~~6A~~7A and ~~Fig. 6B~~7B) illustrate the abundance and proportions of key nitrogen

721 cycle genes in groundwater samples (P-7, P-16, P-20, and P-23) before and after incubation. ~~Figure~~

722 ~~6A~~(A) shows the relative abundance of genes involved in nitrification (archaeal *amoA*, bacterial

723 *amoA*), denitrification (*nirK, nirS, nosZI, nosZII*), nitrogen fixation (*nifH*), and DNRA (*nrfA*), as

724 well as complete nitrification (*commamox*) alongside microbial population markers (archaeal and

725 bacterial 16s rRNA~~). Figure 6B~~)and (B) presents the proportions of these functional genes relative

726 to total prokaryotic abundance, highlighting their contributions to the microbial community

727 structure.

728

729 **4 Discussion**

730 **4.1 Initial groundwater samples – N transformations occurring in field conditions**

731 ~~For identification of possible~~To identify N-~~transformations~~transformation processes occurring

732 naturally in the aquifer, the isotope signatures of inorganic N (NO_3^- and NO_2^-) were compared

733 with the literature-based reference data ~~on~~for denitrification (Fig. 3A) and nitrification (Fig. 3B).

734

735 <u>**4.1.1 Interplay of Denitrification and Nitrification Processes**</u>

736 Figure. 3A illustrates ~~the isotopic composition ($\delta^{15}N$ and $\delta^{18}O$) of NO_3^- in groundwater samples,~~

737 ~~highlighting~~ both the sources of nitrate and the processes that transformed it during the residence

738 time in the aquifer. ~~Samples in the pink-shaded zone reflect NO_3^- contributions from sources such~~

739 ~~as fertilizers, sewage, and soil organic matter decomposition, with minimal microbial~~

740 ~~transformation. Samples with enriched $\delta^{15}N$ and $\delta^{18}O$ values, located in the red-shaded "Residual~~

741 ~~Substrate" zone, indicate advanced denitrification, where residual nitrate is enriched in ^{15}N and~~

742 ~~^{18}O due to preferential reduction of light isotopes. The green shaded area represents NO_2^-~~

743 ~~produced from NO_3^- reduction during partial denitrification, an intermediate step in denitrification.~~

744 ~~The isotopic patterns in the graph also differentiate between autotrophic and heterotrophic~~

~~denitrification. Samples aligning with autotrophic denitrification indicate the reduction of NO_3^-~~
~~coupled with the oxidation of inorganic compounds like sulfur or hydrogen, resulting in a slower~~
~~rate of isotopic fractionation and less pronounced enrichment in $\delta^{15}N$ and $\delta^{18}O$ (Cui et al., 2019;~~
~~Hu et al., 2024). In contrast, samples reflecting heterotrophic denitrification show rapid isotopic~~
~~fractionation due to the use of organic carbon as the electron donor, leading to greater enrichment~~
~~of $\delta^{15}N$ and $\delta^{18}O$ in the residual nitrate (after (Deb et al., 2024)).~~

~~Our~~The isotope values indicate organic matter as the dominant nitrate source and the reductive
trend for nitrate samples. However, the observed denitrification ~~NO_3^- samples (orange triangles,~~
~~Fig. 3A) are located in the area typical for NO_3^- originating from organic matter decomposition~~
~~and of sewage origin. The precise knowledge of the $\delta^{15}N$ signature of the potential N substrates,~~
~~i.e. of DON and waste waters, could further confirm the dominant source of the samples (Boumaiza~~
~~et al., 2024). The nitrate samples present a clear correlation between $\delta^{18}O$ and $\delta^{15}N$ values, typical~~
~~for isotope enrichment due to heterotrophic denitrification leading to ^{18}O and ^{15}N enriched of the~~
~~residual NO_3^-. However, this~~ enrichment is relatively low and the samples do not show typically
high δ values (Fig. 3A). This indicates that the nitrate pool might be constantly renewed with fresh
substrate of low δ values. This suggests active nitrification processes which is reinforced with the
gene abundances observed in field samples, before incubation, Fig. 7, where the majority of gene
copy numbers represent archaeal *amoA*, while denitrification genes occurrence is very low. Hence,
we probably have intensive nitrate production by nitrification processes (Fig. 3B).
~~Our NO_2^- samples (green circles, Fig. 3A), are mostly shifted towards lower $\delta^{15}N$ values, with the~~
~~expected isotope effect typical for denitrification NO_3^- reduction to NO_2^-, with isotopically~~
~~depleted NO_2^- due to the preferential reduction of light isotopes (^{14}N and ^{16}O). $\delta^{18}O_{NO2}$ values are~~
~~similar or lower than the respective NO_3^- source, which may indicate additional incorporation of~~
~~water into the formed NO_2^-.~~
~~Figure .3B illustrates the isotopic composition of nitrate (NO_3^-) and nitrite (NO_2^-) in groundwater~~
~~samples in regard to possible nitrification processes. Autotrophic nitrification, with NO_3^- produced~~
~~from NH_4^+ or organic nitrogen, is characterized by lower $\delta^{15}N$ and $\delta^{18}O$ values, while heterotrophic~~
~~nitrification contributes to NO_3^- and NO_2^- production with distinct isotopic enrichment from~~
~~organic nitrogen compounds. Our NO_3^- samples are located between values typical for NO_3^-~~
~~production from autotrophic and heterotrophic nitrification, the observed correlation might be a~~
~~mixing between these two NO_3^- origins. However, from the NO_2^- samples only two points indicate~~
~~typical values for autotrophic nitrification, whereas others show much lower $\delta^{15}N$ values (Fig. 3B).~~

Both graphs (Fig. 3A and 3B) show the potentially occurring processes, it is important to review
them jointly with the basic aquifer information and further microbial analyses and incubation
studies. The physicochemical parameters for our aquifer present redox conditions theoretically
allowing for occurrence of both denitrification and nitrification processes. (Wolters et al.,
2022)(Brettar et al., 2002). Archival field measurements indicated that the aquifer shows slightly
sub-oxic conditions (section 2.1). Oxygen concentrations in the range of less than 1 and up to 2 mg
O_2 L^{-1} are regarded as the boundary between nitrate-reducing and non-nitrate-reducing conditions
in groundwater (Wolters et al., 2022). Hence, the range of dissolved oxygen content observed for
the aquifer under study of 2.2 - 4.3 mg O_2 L^{-1} is slightly higher, and denitrifying processes might
be suppressed. The redox potential of our aquifer of 213-345 mV lies also on the edge of typical

788 denitrifying conditions from 10 to 300 mV (Brettar et al., 2002). This suggests that reduction

789 processes might occur but might be also accompanied by oxidation processes. Consequently, both

790 conclusions drawn from the Fig. 3A and 3B might be simultaneously true. Whereas NO_3^- is being

791 denitrified it might be simultaneously produced both in autotrophic and heterotrophic nitrification,

792 which ~~is supported by~~results in only small NO_3^- enrichment~~.~~ in heavy isotopes. Groundwater

793 samples of dominant denitrification typically show much higher NO_3^- isotope signatures (Clague

794 et al., 2019).

795 Similarly, NO_2^- isotopic signature shows most probably a mixture of NO_3^- reduction and its

796 formation due to nitrification, in various proportions for different samples. There is one sample of

797 the highest $\delta^{18}O_{NO2}$ and $\delta^{15}N_{NO2}$ (Fig. 3B). This is the P-L2-1 piezometer located closest to the

798 lagune of yeast sewage storage, the sample of the highest NH_4^+ content (Table ~~1~~S1). In this sample

799 NO_2^- must originate mostly from autotrophic nitrification from ammonium oxidation, as it can be

800 concluded from Fig. 3B.

801 ~~The conclusion of~~ Although the isotope signatures provide strong evidence for active

802 denitrification and mixed nitrification pathways in the aquifer, it is important to acknowledge that

803 these isotope-based interpretation of NO_3^- and NO_2^- transformations are based on single-timepoint

804 groundwater sampling in open aquifers. Therefore, processes ~~is reinforced~~such as water exchange,

805 nutrient diffusion, and variations in nitrogen transformation may also influence the observed

806 isotopic signatures and cause their significant changes in time.

807

808 **4.1.2. Actual N sources and transformations**

809 The increased concentrations of both DON and NO_3^- in most piezometers suggest that organic

810 nitrogen input may contribute to higher NO_3^- concentration. Although direct groundwater flow

811 paths were not explicitly studied, the spatial positioning of these wells to the lagoon, along with

812 ~~the gene abundances observed in field~~their elevated DON levels, supports the possibility of

813 influence from wastewater discharge. The precise knowledge of the $\delta^{15}N$ signature of the potential

814 N substrates, i.e. of DON and waste waters, could further confirm the dominant source of the

815 samples~~, before incubation, Fig. 6, where the majority of gene copy numbers represent archaeal~~

816 ~~amoA, while denitrification genes occurrence~~ (Boumaiza et al., 2024).

817 Interestingly, the NH_4^+ content is very low~~. Hence, we rather have intensive nitrate production by~~

818 in the piezometers of high NO_3^- content (Tab. S1) indicating its rapid nitrification. Most possible

819 explanation suggests microbial mineralization of DON to NH_4^+, with instantaneous rapid

820 nitrification to NO_3^- under suboxic conditions. A few piezometers with elevated NH_4^+ content

821 show very low NO_2^- and NO_3^- contents, which may suggest that the nitrification processes ~~(Fig.~~

822 ~~3B).~~are not active there. However, these waters were not selected for further incubation studies,

823 due to our focus on NO_3^- formation and the selection of NO_3^--rich waters. Future studies should

824 integrate groundwater level measurements or tracer-based studies to confirm source connectivity

825 between lagoons and piezometers, along with sampling of NH_4^+-rich, NO_3^--poor locations for

826 better analysis of nitrogen transformation pathways.

827 ~~To further figure out which potential N transformations are active in the aquifer we performed the~~

828 ~~laboratory incubations in controlled conditions of selected water samples.~~

4.2 Active N transformation processes during incubation

4.2.1. Inorganic ~~N analyses~~nitrogen dynamic

The dynamic variations in inorganic N concentration and isotopic evolution of NO_3^- and NO_2^- during the laboratory incubation experiments (Fig. 4) across all incubated samples (P-7, P-16, P-20, and P-23) reflects active microbial transformations during the incubation period.

(A) Phase I (Pre-Glucose addition) : NO_3^- reduction and NO_2^- accumulation

Prior to glucose addition, the observed decrease in NO_3^- concentration, coupled with a parallel increase in $\delta^{18}O_{NO_3}$ and $\delta^{15}N_{NO_3}$ (Fig.4), suggests intensive denitrification with preferential reduction of light isotopes resulting in enrichment of the residual nitrate. According to (Kendall et al., 2007; Kendall and Aravena, 2000) a parallel decrease in NO_3^- concentration and increase in $\delta^{15}N$–NO_3^- is characteristic of denitrification which allows estimation of nitrogen isotope enrichment factor and helps quantify microbial NO_3^- reduction. The apparent isotope effect, i.e. the difference between the initial and final (after 7 days) NO_3^- isotope signature is from 20 to 33‰ for $\delta^{15}N_{NO3}$ and from 12 to 18‰ for δ^{15}~~N_{NO3}~~O_{NO3} giving O/N ratio from 0.45 to 0.83, which is typical slope for heterotrophic denitrification (from 0.48 to 0.88) (Boumaiza et al., 2024; Clague et al., 2019).

During this first phase the NO_2^- concentration clearly increase from near 0 to a few mg NO_2^- L^{-1} and $\delta^{15}N_{NO_2}$ values show slight increase (Fig.4). This shows that the elevated $\delta^{15}N_{NO3}$ (due to low-level labeling) is only partially transferred to the NO_2^- pool. However, the low magnitude of this increase is rather surprising, i.e., the δ^{15}~~N_{NO_2}~~N_{NO2} do not approach the high $\delta^{15}N_{NO3}$ values ~~of NO_3^-,~~, but increase only slightly. This indicates that the formed nitrite must partially originate from another ^{15}N-depleted pool (unlabelled). Isotope-based calculations (Section 3.1.3) indicated that most of the NO_2^- produced during incubation did not originate from NO_3^- reduction, but instead likely derived from an unlabelled nitrogen pool (80 to 95%, Table 1).~~Based on the observed $\delta^{15}N_{NO3\_0}$ (initial value, day 0) and change in $\delta^{15}N_{NO2}$ values (between day 0 and day 7 of the incubation) we can calculate the maximal contribution of NO_2^- originating from NO_3^- reduction (NAR) in this new-formed NO_2^- applying the isotope mass balance (Eq.1). These calculations are simplified by neglecting any isotope fractionation of the NO_2^- pool.~~

$$NAR = \frac{\delta^{15}N_{NO2-7} - \delta^{15}N_{NO2-0}}{\delta^{15}N_{NO3-0}} \quad \text{(Eq.1)}$$

~~**Table 4: Inputs and results of the mass balance calculations for determining the contribution of nitrate reduction (NAR) in the nitrite pool** with Eq.1: $\Delta\delta^{15}N_{NO_2}$ is the change of nitrite N isotope signature between day 0 and day 7, $\delta^{15}N_{NO3-0}$ – initial N isotope signature of nitrate, Δ [NO_2^-], is the change of nitrite concentration between day 0 and day 7, mg/L NAR is the amount of produced nitrite originating from NAR, Δ [NO_3^-] is the nitrate consumption between day 0 and day 7.~~

~~Piezometer~~	~~$\Delta\delta^{15}N_{NO_2}$~~	~~$\delta^{15}N_{NO3-0}$~~	~~NAR [%]~~	~~Δ [NO_2^-] mg N L^{-1}~~	~~mg/L NAR~~	~~Δ [NO_3^-] mg N L^{-1}~~
~~P-7~~	~~33.1~~	~~192.2~~	~~17.2~~	~~7.3~~	~~1.3~~	~~-13.7~~

P-16	18.1	207.1	8.7	13.4	1.2	-23.0
P-20	13.4	306.5	4.4	3.6	0.2	-17.2
P-23	14.1	69.0	20.4	6.1	1.2	-33.2

868

869 The calculation results (Table 4) indicate that from 0.2 up to 1.3 mg N-NO$_2^-$ L^{-1} originates from
870 NAR, which is low amount when compared to the magnitude of N-NO$_3^-$ consumption of 13.7 to
871 33.2 mg L^{-1} (Table 4). This agrees with the fact that NO$_2^-$ is a very reactive and short-living
872 compound and as denitrification intermediate it instantaneously undergo further reduction
873 (Lewicka-Szczebak et al., 2021). But interestingly, the large majority of N-NO$_2^-$ (80 to 95 %)
874 originates from other transformations than NO$_3^-$ reduction. Since the NH$_4^+$ contents are very low
875 in all the samples, this unlabelled N source for NO$_2^-$ production must originate from dissolved
876 organic N (DON). This pathway is very plausible since the samples show high DON contents from
877 31 to 92 mg N L^{-1} (Table 2). For most samples, NO$_2^-$ show significant increase in $\delta^{18}O_{NO_2}$ values
878 in the first phase (between day 0 and day 7), indicating that the major source of O must be
879 molecular O$_2$ with characteristic high $\delta^{18}O_{O_2}$ of +23.5‰ (Moore et al., 2006). Since S2). The
880 application of yeast-based sewage as fertilizer in the agricultural site likely introduced organic
881 nitrogen into the groundwater, which undergoes microbial decomposition to release ammonium
882 (NH$_4^+$) through the mineralization of proteins and amino acids (Watanabe et al., 2023). However,
883 NH$_4^+$ contents were very low during all the incubations applied suboxic atmosphere (up to 5% in
884 the headspace and 2.1 mg of dissolved oxygen (Table 2),(Fig. 4), indicating its rapid
885 transformation within the nitrogen cycle, such as nitrification and assimilation. Microbial
886 assimilation likely contributed to NH$_4^+$ exhaustion, as microbes utilized it for biomass synthesis.
887 However, this low amounts of oxygen must have been used or the oxygen must had been fixed
888 before in other compounds, like organic matter, and further used is not the case for oxidation
889 processes. Only for P-23 the $\delta^{18}O_{NO_2}$ value stays stable, this sample shows most intensive NO$_3^-$
890 reduction due to denitrification and most probably the potential increase was masked with O-atoms
891 exchange between water and denitrification intermediates (Lewicka-Szczebak et al., 2016). sterile
892 samples, where we observe slight accumulation of NH$_4^+$, indicative of biological uptake in NH$_4^+$
893 turnover.

894

895 **(B) Phase II (Post-Glucose addition) : Chemodenitrification and possible nitrification**
896 In the second phase of the incubation, after glucose addition, further NO$_3^-$ reduction was observed
897 in all samples (Fig. 4A). However, despite this observed reduction, δ value stay stays quite stable,
898 with much less isotope enrichment between day 7 and 14 of the incubation, when compared to the
899 day 0 - day 7 enrichment, both for $\delta^{15}N$ and $\delta^{18}O$ (Fig. 4B). Hence, we do not observe here the
900 typical isotope enrichment characteristic for denitrification processes (Boumaiza et al., 2024). The
901 However, the occurrence of intensive denitrification during the second incubation phase can be
902 clearly proved with N$_2$O data, which show high ^{15}N content, and $\delta^{15}N^{SP}$ and $\delta^{18}O$ values typical
903 for bacterial denitrification (Fig. 56). Also the analysed gene abundances clearly indicate
904 intensification of denitrification genes during the incubation (Fig. 67). But despite active
905 denitrification process, the typical isotope enrichment of the residual NO$_3^-$ is not observed. This

might possibly indicate significant additional contribution of other process of nitrate reduction. Chemodenitrification can be considered, since this process is associated with no kinetic isotope effects for either $\delta^{15}N$ or $\delta^{18}O$ in the residual NO_3^- pool (~~(X.~~ Wang et al., 2022). This assumption can be reinforced with the sterile samples data, where nitrate pool is also largely reduced (Fig. 4A) without any isotope effects (Fig. 4B). This indicates that the conditions in the studied groundwaters may support chemodenitrification.

Simultaneously, $\delta^{15}N_{NO_2}$ mostly go down or increase only slightly, indicating that the transformations of unlabelled N source are getting even more active than in the first incubation phase and there is nearly no detectable contribution of NO_2^- from NO_3^- reduction. However, the labelled ^{15}N is present in the further denitrification product – N_2O~~,~~ (Fig. 6), hence it must have been transformed through NO_2^- as the first denitrification intermediate. This shows that this conversion takes place very rapidly, maybe even in the same microbial cell and NO_2^- must be nearly completely converted to further denitrification products. This agrees with the fact that NO_2^- is a very reactive and short living compound and as denitrification intermediate it instantaneously undergoes further reduction (Lewicka-Szczebak et al., 2021).

Importantly, the common pool of NO_2^-, which do not show ^{15}N enrichment, is mostly not converted to N_2O. This is proven by the fact that $\delta^{15}N_{N2O}$ values are very close to $\delta^{15}N_{NO3}$, but much higher than $\delta^{15}N_{NO2}$ during the second incubation phase. Hence, the NO_2^- newly formed in nitrification processes is not further reduced to N_2O but is most probably rather further oxidised to NO_3~~,~~. Since this process would add ^{15}N depleted NO_3^- this can mask the ^{15}N enrichment due to denitrification. In this second incubation phase, O isotope signatures of NO_2^- and NO_3^- mostly move towards each other, which indicates probably intensive reversible reactions of reduction and oxidation between these two compounds, which facilitates O-atoms exchange with water. This agrees with the recent findings by (Zheng et al., 2023) who indicated tighter cycling between these both compounds with particular importance of NO_2^- re-oxidation processes. The inconsistencies found in our data for ^{15}N content in NO_3^-, NO_2^- and N_2O pool ~~reinforces~~ reinforce the assumption of separate NO_2^- pools for particular N transformation pathways (Müller et al., 2014; Rütting and Müller, 2008; Zhang et al., 2023). Although most of these previous studies apply for soils, it is apparently also true for groundwater N transformations.

~~A closer look on the~~

(C) NO_2^- production pathways: Phase I and II

Before the addition of glucose, the nitrite isotopic ~~analysis of nitrite (NO_2^-) in the groundwater incubation study~~ signatures (Fig. ~~7) reveals that the highest nitrite concentrations are characterised by the lowest isotope signatures. We observe a statistically significant correlation between O and N isotopic signatures of NO_2^-. Theoretically, this could be the mixing line with the ^{15}N labelled values originating from labelled NO_3^-, reduction, but this NO_3^-, shows low $\delta^{18}O$ values in the range from -16 to +10‰. Hence, this rather shows mixing of the different origins of unlabelled NO_2, which is in great majority (as shown above and in Table 4), potentially originating from~~ 5) were mostly associated with heterotrophic nitrification zone, suggesting a mix of both autotrophic and heterotrophic ~~nitrification processes.~~

~~within the nitrogen cycle. The absence of NH_4^+ can be attributed to its immediate consumption through~~ Following glucose addition, the nitrite isotopic signatures (Fig.5) were more concentrated within the autotrophic nitrification zone, which indicates that autotrophic nitrification~~, where ammonia is oxidized to NO_2^- and NO_3^-. The clustering of isotopic data within the autotrophic nitrification zone in Fig. 7 before glucose addition supports this process, highlighting ammonia oxidation as a dominant pathway. Additionally, microbial assimilation likely contributed to NH_4^+ exhaustion, as microbes utilized it for biomass synthesis. This is not the case for sterile samples, where we observe slight accumulation of NH_4^+.~~

~~Following glucose addition, the isotopic signatures (filled circles) become more dispersed, with several data points shifting~~ continued to dominate nitrite production despite under elevated carbon conditions. While a shift towards ~~the~~ heterotrophic nitrification ~~zone. This shift suggests that glucose addition stimulated heterotrophic bacteria, altering nitrite production pathways. While autotrophic nitrification likely continued, the spread in isotopic values indicates that heterotrophic nitrifiers also contributed to nitrite production, likely utilizing organic nitrogen compounds, supporting a transition from predominantly autotrophic to mixed nitrification processes.~~ might be expected under increased carbon availability, the isotope data suggest that autotrophic ammonia-oxidizing bacteria remained more metabolically active than the heterotrophs under the given incubation conditions. Together, these findings demonstrate the rapid transformation of NH_4^+ from yeast-based fertilizers into intermediate nitrogen compounds, driving nitrification and subsequent nitrogen cycling processes in groundwater.

For most samples, NO_2^- shows significant increase in $\delta^{18}O_{NO_2}$ values in the first phase (between day 0 and day 7), indicating that the major source of O must be molecular O_2 with characteristic high $\delta^{18}O_{O_2}$ of +23.5‰ (Moore et al., 2006), which is plausible in the suboxic atmosphere applied (up to 5% in the headspace and 2.1 mg of dissolved oxygen (Table S2)), .Only for P-23 the $\delta^{18}O_{NO_2}$ value stays stable, this sample shows most intensive NO_3^- reduction due to denitrification and most probably the potential increase was masked with O-atoms exchange between water and denitrification intermediates (Lewicka-Szczebak et al., 2016).

4.2.2 Gene Abundance Shifts in Microbial Communities

The gene abundances before incubation indicate strong nitrification potential (Fig. 7). This is consistent with findings from (Mosley et al., 2022), which reported that ammonia-oxidizing archaea (AOA) tend to dominate in oligotrophic groundwater environments with low ammonia concentrations due to their higher affinity for ammonia and oxygen limitation, often outnumbering ammonia-oxidizing bacteria (AOB). Similarly, the functional gene proportion analysis (Fig. 7B) highlight the contribution of archaeal *amoA* genes to total prokaryotic abundance, emphasizing their critical role in ammonia oxidation.. In contrast, the low proportions of bacterial *amoA* further confirm limited bacterial involvement in N cycling prior to incubation. This has also been observed in groundwater systems where bacterial nitrification potential remains constrained due to environmental limitations on AOB populations.

The observed post-incubation shift towards increasing denitrification potential aligns with (Wang et al., 2022), who found that site-specific environmental conditions, particularly carbon and N availability drive microbial community shifts in N cycling, with increased denitrification gene

33

abundance. Functional gene proportions also reveal a corresponding rise in the relative abundance of *nosZI*, illustrating the shift in microbial community function towards denitrification processes Fig. 7B. The abundance of DNRA and commamox genes showed minimal changes, suggesting no difference in the presence of these processes between pre- and post-incubation conditions. This observation is consistent with (Broman et al., 2021), who reported that DNRA gene abundance remained stable under experimental conditions, indicating its potential resilience to shifts in N cycling pathway.

These dynamic microbial changes indicate that specific environmental or experimental conditions during incubation can significantly influence certain microbial processes, particularly those related to N cycling. This is consistent with (Wang et al., 2022), who found N-cycling gene abundance varies with environmental factors like carbon and N availability. Similarly, (Mosley et al., 2022) reported persistent transcriptional activity in nitrification and denitrification across groundwater conditions, indicating microbial adaptability. The significant results for the community of *nosZI* and archaeal 16s rRNA highlight their potential roles in environmental monitoring and microbial ecology studies.

The observed variations across the piezometers after glucose addition were not uniform and can be attributed to site-specific conditions such as initial nitrate concentrations, DON levels, and also variation in microbial communities. Notably, *nosZI* gene abundance increased across all piezometers, with higher enrichment in P-16 and P-20, and suggests enhanced denitrification potential. Conversely, archaeal *amoA* gene abundance declined—particularly in P-7 and P-23—indicating a microbial shift from archaeal-driven nitrification to bacterial denitrification. These patterns highlight how suboxic, carbon-rich conditions can selectively enhance denitrification, depending on environmental conditions.

4.2.2 Headspace3. N₂O analyses and FRAME isotope modelproduction pathways

(A) Microbial N₂O sources: Phase I and II

Thanks to the application of low-level labelling strategy the source isotopic signatures for N_2O production pathways can clearly distinguish between nitrification processes, which utilize the non labelled NH_4^+ pool, and denitrification processes, which must result in $\delta^{15}N$ enrichment due to ^{15}N enriched NO_3^- substrate (Fig. 6). Both from the samples location on the isotope maps (Fig. 6) and from the FRAME modelling results we observe the significant contribution of nitrification processes in the first samples and very clear dominance of the bacterial denitrification in the Phase II of the incubation (Fig. S1).

The FRAME analysis of N₂O isotope data, T-test results, and gene abundance graphs together show a shift from nitrification to denitrification in microbes during incubation, influenced by addition of carbon source and suboxic conditions. Initially, the FRAME results show that nitrification, mainly due to archaeal community (as seen with high levels of the archaeal *amoA* gene), is the dominant N₂O production pathway. Isotope analysis supports this, with N₂O isotope signatures characteristic for nitrification for the first samples (Fig. 6, Fig. S1). Pre-incubation data

indice that archaeal ammonia oxidation was a dominant process in samples P-7 and P-20, as evidenced by higher archaeal *amoA* gene abundance relative to denitrification-related genes. However, in samples such as P-16 and P-23, the abundance of *nosZI* suggests that denitrification processes were also active, pointing to a co-occurrence of nitrification and denitrification processes across the groundwater samples.

Post-incubation, FRAME results show an increase in bacterial denitrification (bD) fractions, correlating with the significant rise in denitrification-related genes, particularly *nosZI* validated by paired T-tests ($p < 0.05$). These changes are confirmed by gene abundance graphs that show a notable increase in these denitrification genes after incubation. The total prokaryotic abundance also increased in P-16 and P-20, reflecting enhanced bacterial growth, whereas smaller changes in P-7 and P-23 suggest variable responses to carbon addition (Fig. 7). A decline in nitrification genes align with the FRAME-predicted reduction in nitrification activity. Additionally, isotopic data revealed significant N_2O reduction to N_2 in most samples, consistent with bacterial denitrification dominance, reduced contributions from nitrification pathways, and increase in the abundance of genes responsible for N_2O reduction to N_2 (*nosZII*). Together, these results confirm microbial transition from archaeal-driven nitrification to bacterial denitrification, highlight the role of carbon availability and suboxic conditions in regulating N cycling. The integration of gene abundance, isotope dynamics, and FRAME analysis provides a comprehensive understanding of the microbial processes driving N transformations during incubation.

All piezometers displayed a similar transition from nitrification-driven processes in the first samples to denitrification-dominated processes in the later incubation days. However, at the final sampling points, no fitted solution could be obtained for some data, suggesting the presence of unknown processes or a complex overlap of microbial pathways. These findings indicate very dynamic N_2O production processes while highlighting limitations in resolving mixed nitrogen pathways at later stages. Figure 5 illustrates the isotopic signatures ($\delta^{15}N^{SP}_{N2O}$, $\delta^{18}O_{N2O}$ and $\delta^{15}N_{N2O}$) of N_2O in headspace samples collected during laboratory incubation with the relevant microbial N transformation pathways presented based on the literature data (Yu et al., 2020) and taking into account the actual measured isotopic signatures of sources applied in this case study ($\delta^{18}O_{H2O}$, $\delta^{15}N_{NO3}$). Before glucose addition (white dots), the isotopic signatures indicate mixing between nitrification and denitrification processes (Fig. 5A). In P-7, before glucose addition, isotopic data clustered near the nitrifier denitrification (nD) zone, highlighting ammonia oxidation and partial N_2O reduction. In P-16, isotope signatures widely distributed between nitrifier and bacterial denitrification zones, suggesting overlapping processes. In P-20 and P-23, clustering near the bacterial denitrification (bD) zone reflected nitrate reduction as the dominant pathway with minimal N_2O reduction.

After glucose addition, the isotopic data indicate that N_2O production was primarily driven by bacterial denitrification (bD), with relatively low $\delta^{15}N^{SP}_{N2O}$ and $\delta^{18}O_{N2O}$ values, clustering mostly around reduction line. In the $\delta^{15}N^{SP}$ – $\delta^{15}N$ space, mostly the isotopic data showed a clear shift toward bD, supported by a significant increase in $\delta^{15}N_{N2O}$ values, indicating N_2O production from the slightly ^{15}N-labeled NO_3^- pool and some effect of N_2O reduction. In P-23, however, the data indicate more possible pathways mixture, including nitrification (Ni) and fungal denitrification (fD). Significant reduction of N_2O to N_2 can be supposed based on the clustering of the points along the N_2O reduction line, especially in the $\delta^{15}N^{SP}$ – $\delta^{18}O$ isotope map, Fig. 5). In $\delta^{15}N^{SP}$ – $\delta^{15}N$ isotope map the effect of N_2O reduction is less visible, because the artificially elevated $\delta^{15}N$ values
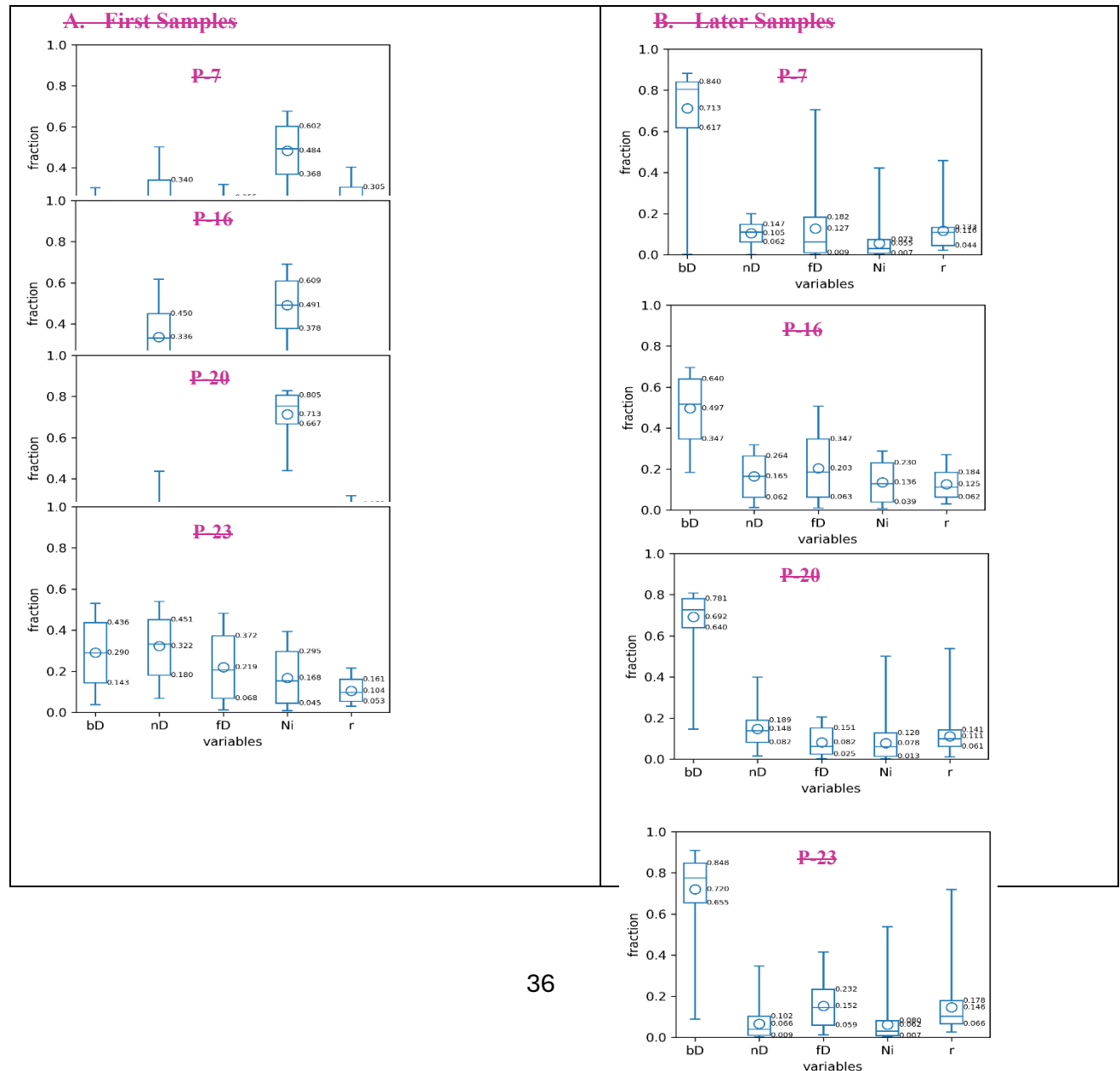
1109
1110
1111

1112

Figure 8: N$_2$O production pathways contribution and N$_2$O reduction progress based on the FRAME modelling of the experimental N$_2$O isotope data collected for the first analysed samples (before glucose addition, 1st and 2nd sampling, day 2 and 4) (A) and mean value of the later samples (after glucose addition, 4th and 5th sampling, day 9 and 11) (B). The estimated contributions of bacterial denitrification (bD), nitrifier denitrification (nD), fungal denitrification (fD), and autotrophic nitrification (Ni) illustrate the dynamic shifts in microbial pathways and N$_2$O reduction progress (r) over time.

The graphs, analyzed using the FRAME model, reveal distinct microbial processes driving N$_2$O production and reduction during laboratory incubation of groundwater samples from piezometers P-7, P-16, P-20, and P-23, comparing the initial incubation phase (1–2 days) to the later phase (4–14 days), including samples before and after glucose addition.

This division of samples was made after the observed isotopic signatures – the initial samples (day 2) showed no ^{15}N enrichment in the N$_2$O and later samples (day 7 – day 14) were characterised with very significant ^{15}N enrichment. Initially, autotrophic nitrification (Ni) dominated across all samples, contributing around 60–70% to N$_2$O production, while bacterial denitrification (bD) was lower, ranging between 20–30%. In P-7 and P-16, minor contributions from nitrifier denitrification (nD) (10–20%) and fungal denitrification (fD) (<10%) were observed, with similar trends in P-20 and P-23, where nD accounted for slightly higher fractions of N$_2$O production. Residual N$_2$O fractions (r$_{N2O}$) across all piezometers ranged between 10–26%, reflecting high partial N$_2$O reduction to N$_2$.

After glucose addition, microbial activity shifted significantly toward denitrification, with bD becoming the dominant pathway (up to 80–85%), driven by the availability of carbon. P-7 and P-16 exhibited a gradual rise in bD, reaching up to 73%, while residual Ni contributions declined correspondingly. In P-20 and P-23, the transition was sharper, with bD dominance occurring more abruptly. Residual N$_2$O fractions decreased across all samples as bD activity intensified. Simultaneously, Ni contributions dropped below 10% in all samples, while nD and fD remained minimal, contributing <15% to N$_2$O production. Interestingly, for the last sample (day 14 of the incubation) for all the analysed waters the model could not find any solution. This might be due to accumulation of very different pathways contribution and progressing reduction of N$_2$O originating from the mixture of all production pathways. Figure 9 presents illustration of the model performance on an example of sample 6 (day 14) of the P-16, while this is similar for all the piezometers. The modelling problem occurs due to too high δ^{18}O measured values, while δ^{15}N and δ^{15}N^{SP} show values typical for bD, δ^{18}O is shifted to much higher values, indicating large reduction, not confirmed with low δ^{15}N^{SP} values. This can result from the actual smaller O-isotope exchange with water than the one assumed by for bD in the model input values.

(B) Abiotic N$_2$O contribution

While microbial denitrification was the primary N$_2$O source, the observed discrepancies suggest that abiotic contributions, such as chemodenitrification, may have been a more relevant factor than initially expected, particularly under conditions favoring nitrite accumulation.

The endmember values for bD are mostly determined based on soil experimental studies (Yu et al., 2020), hence it is theoretically possible that slightly different range of values should be assumed for groundwater studies. Another explanation could be a significant admixture of chemodenitrification pathway, which is characterized by high $\delta^{18}O$ values ((Wei et al., 2019). This assumption might be supported by the fact that quite significant N_2O production was found in some of sterile samples, with especially high production at the end of the experiment (Table 2S2). This N_2O produced from sterile treatments shows always high $\delta^{18}O$ values and very variable $\delta^{15}N^{SP}$ values (Fig. 5A).6A). This highlights the importance of considering abiotic N_2O formation, especially under low-oxygen conditions. Similarly, previous studies showed distinct isotope fractionation patterns for N_2O production due to chemodenitrification, including elevated $\delta^{18}O$ values compared to microbial pathways (Chen et al., 2021).

This interpretation is further supported by the elevated $\delta^{18}O$ values in later incubation stages, suggesting abiotic processes like chemodenitrification which may have contributed to N_2O production. Chemodenitrification has been shown to produce N_2O with distinct isotope fractionation patterns, including elevated $\delta^{18}O$ values compared to microbial pathways (Chen et al., 2021). The detection of N_2O in sterile samples alsoThe detection of N_2O in sterile samples points to a possible non-biological contribution, as nitrite can undergo chemical reduction in the absence of microbial activity (Heil et al., 2016). Furthermore, abiotic N_2O formation has been linked to Fe(II)-mediated nitrite reduction, particularly under anoxic conditions, with organic matter, including humic and fulvic acids, potentially facilitating N_2O production through chemical pathways (Zhu-Barker et al., 2015). However, since Fe(II) presence in our sterile samples is unknown, other abiotic mechanisms, such as organic matter interactions, cannot be ruled out. Importantly, the FRAME model does not include chemodenitrification, which is most probably the reason for biased results for the last samples. The discrepancies between modeled and observed isotope values (Fig. S2) suggest that additional abiotic pathways, such as chemodenitrification, may need to be considered in future isotope models to improve accuracy.
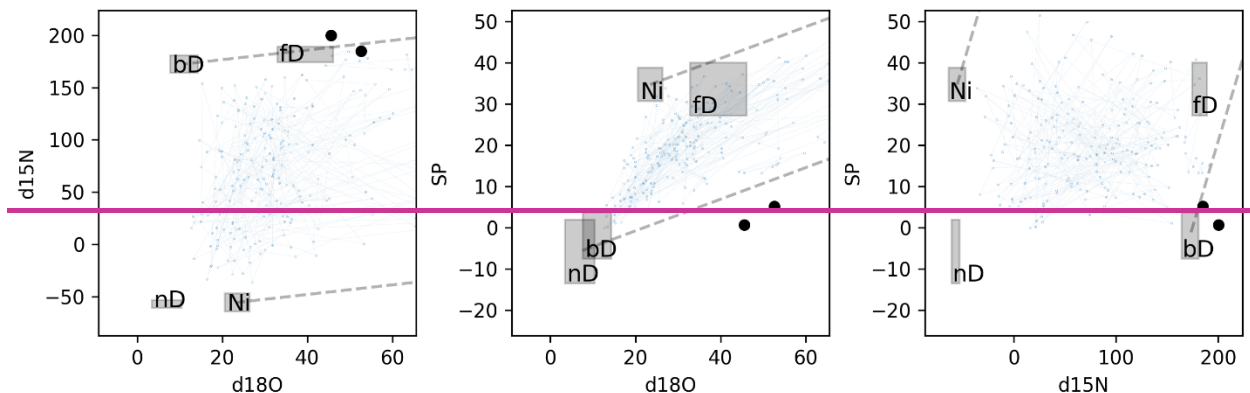

Figure 9: An example of the FRAME modelling path illustration for the last incubation samples (P-16, day 14), which do not provide modelling results. The black dots illustrate

measured samples and the blue points the model Monte Carlo sampling. No coherence of measured and modelled data indicate that the model did not find plausible solution for the given data.

All piezometers displayed a similar transition from nitrification-driven processes in the first samples to denitrification-dominated processes in the later incubation days. However, at the final sampling points, no fitted solution could be obtained for some data, suggesting the presence of unknown processes or a complex overlap of microbial pathways. These findings indicate very dynamic N₂O production processes while highlighting limitations in resolving mixed nitrogen pathways at later stages. Moreover, while microbial denitrification was the primary N₂O source, the observed discrepancies suggest that abiotic contributions, such as chemodenitrification, may have been a more relevant factor than initially expected, particularly under conditions favoring nitrite accumulation.

4.2.3 Gene Abundance Shifts in Microbial Communities

Pre-incubation data indicate a notable presence of aarchaeal *amoA* genes compared to bacterial *amoA,* suggesting active archaeal ammonia oxidation in the samples (Fig. 6A). While denitrification gene *nosZI* show relatively high abundance in some samples (e.g., P-16 and P-23), the consistent presence of archaeal *amoA* and the lower abundance of other denitrification-related genes (*nirK, nirS,*), , suggests nitrification processes were prominent prior to incubation. This is particularly evident in P-7 and P-20, where archaeal *amoA* surpasses denitrification genes, suggesting a stronger nitrification potential.

This is consistent with findings from (Mosley et al., 2022), which reported that ammonia-oxidizing archaea (AOA) tend to dominate in oligotrophic groundwater environments with low ammonia concentrations due to their higher affinity for ammonia and oxygen limitation, often outnumbering ammonia-oxidizing bacteria (AOB). Similarly, the functional gene proportion analysis (Fig. 6B) highlight the contribution of archaeal *amoA* genes to total prokaryotic abundance, emphasizing their critical role in ammonia oxidation.. In contrast, the low proportions of bacterial *amoA* further confirm limited bacterial involvement in N cycling prior to incubation. This has also been observed in groundwater systems where bacterial nitrification potential remains constrained due to environmental limitations on AOB populations. Post-incubation, there was a significant increase in the abundance of denitrification genes like *nosZI,* particularly in samples P-7, P-16 and P-20, illustrating a shift from nitrification to denitrification under incubation conditions Fig. 6(A). This aligns with (Wang et al., 2022), who found that site-specific environmental conditions, particularly carbon and N availability drive microbial community shifts in N cycling, with increased denitrification gene abundance. Functional gene proportions also reveal a corresponding rise in the relative abundance of *nosZI,* illustrating the shift in microbial community function towards denitrification processes Fig. 6(B). The abundance of DNRA and commamox genes showed minimal changes, suggesting no difference in the presence of these processes between pre- and post-incubation conditions. This observation is supported by (Broman et al., 2021), who reported that DNRA gene abundance remained stable under experimental conditions, indicating its potential resilience to shifts in N cycling pathway. The abundance of archaeal 16S rRNA genes decreased in samples P-7 and P-23, indicating a reduction in archaeal community, whereas the abundance of bacterial 16S rRNA increased significantly in P-16 and P-20, reflecting bacterial growth during incubation. Paired T-tests confirmed these observations, showing significant increases in the

~~abundance of *nosZI* genes in P7 (p<0.05) and P16 (p<0.05) and shifts in the archaeal 16S rRNA~~
~~abundance (p<0.05), but not in the abundances of *nirK* or *nosZII* genes (p>0.05), highlighting the~~
~~variability in microbial responses.~~ ~~These results suggest that specific environmental or~~
~~experimental conditions during incubation can significantly influence certain microbial processes,~~
~~particularly those related to N cycling. This is consistent with (Wang et al., 2022), who found N-~~
~~cycling gene abundance varies with environmental factors like carbon and N availability.~~
~~Similarly, (Mosley et al., 2022) reported persistent transcriptional activity in nitrification and~~
~~denitrification across groundwater conditions, indicating microbial adaptability.~~ ~~The significant~~
~~results for the community of *nosZI* and archaeal 16s rRNA highlight their potential roles in~~
~~environmental monitoring and microbial ecology studies.~~

4.2.4 The identification of active N transformations in the laboratory incubations

The interpretation of the presented results is quite challenging, since this is the first study combining the N and O isotope analyses of NO_3^- and NO_2^- as well as N_2O isotopes including three signatures: $\delta^{15}N^{SP}_{N2O}$, $\delta^{18}O_{N2O}$ and $\delta^{15}N_{N2O}$. The overall summary of this data is rather surprising and may seem inconsistent, because the low-level ^{15}N label added to the NO_3^- pool is not found in the NO_2^- pool, but almost completely transferred to the N_2O pool. Both the N_2O isotope results and gene copy numbers document occurrence of intensive denitrification, especially in the second phase of the incubation, whereas the analyses of inorganic N indicate simultaneous intensive nitrification processes, with significant formation of NO_2^-~~.~~ . It is surprising due to very low levels of NH_4^+ during the whole incubation and indicates that the additional unlabelled N must originate from organic nitrogen pool (DON~~). -~~) and the intermediately formed NH_4^+ is rapidly further nitrified to NO_2^- and NO_3^- .

~~The FRAME analysis of N_2O isotope data, T-test results, and gene abundance graphs together~~
~~show a shift from nitrification to denitrification in microbes during incubation, influenced by~~
~~adding carbon source and created suboxic conditions.~~ ~~Initially, the FRAME results show that~~
~~nitrification, mainly due to archaeal community (as seen with high levels of the archaeal *amoA*~~
~~gene), is the dominant N_2O production pathway. Isotope analysis supports this, with N_2O isotope~~
~~signatures characteristic for nitrification for the first samples (Fig. 5, Fig.8). Pre-incubation data~~
~~indicate that archaeal ammonia oxidation was a dominant process in samples P-7 and P-20, as~~
~~evidenced by higher archaeal *amoA* gene abundance relative to denitrification-related genes.~~
~~However, in samples such as P-16 and P-23, the abundance of *nosZI* suggests that denitrification~~
~~processes were also active, pointing to a co-occurrence of nitrification and denitrification processes~~
~~across the groundwater samples.~~

~~Post-incubation, FRAME results show an increase in bacterial denitrification (bD) fractions,~~
~~correlating with the significant rise in denitrification-related genes, particularly *nosZI* validated by~~
~~paired T-tests (p<0.05). These changes are confirmed by gene abundance graphs that show a~~
~~notable increase in these denitrification genes after incubation. The total prokaryotic abundance~~
~~also increased in P-16 and P-20, reflecting enhanced bacterial growth, whereas smaller changes in~~
~~P-7 and P-23 suggest variable responses to carbon addition (Fig. 6). A decline in nitrification genes~~
~~align with the FRAME-predicted reduction in nitrification activity. Additionally, isotopic data~~

Importantly, the overall results showed that both reduction and oxidation processes are occurring simultaneously in the studied aquifer. Theoretically, in our incubations the suboxic conditions should rather favor denitrification NO_3^- reduction. Indeed, the majority of the released N₂O is formed due to bacterial denitrification from NO_3^- as a substrate. However, NO_2^- originate in large majority from organic N oxidation with very minor fraction originating from NO_3^- reduction. These results suggest that in groundwater systems impacted by agricultural or wastewater-derived organic matter, DON can significantly contribute to nitrite formation under suboxic conditions, alongside microbial denitrification and influencing nitrogen transformation pathways. To stimulate microbial denitrification under suboxic conditions, glucose was added as a carbon source. This approach is also supported by previous research (Liu et al., 2022) where external carbon addition, significantly enhanced biological denitrification and nitrate removal efficiency in groundwater. This helps understand how elevated organic carbon (e.g., from wastewater or agricultural leachate) could influence N-transformations in the field. In our study, the observed shift from archaeal-driven nitrification to bacterial denitrification highlights the role of carbon availability in nitrogen cycling pathways. While lab incubations cannot fully mimic the complex field-scale conditions, they provide insights into microbially mediated processes. Future in situ studies incorporating natural carbon amendments would help validate these findings under real, open-system aquifer conditions.

4.2.5. Comparability of laboratory incubation and field groundwater studies

Laboratory incubation studies are typically conducted under controlled, closed-system conditions for detailed investigation of specific nitrogen transformation pathways and quantify isotopic and microbial changes without external mass exchange. However, applying the results to natural groundwater systems —which may often have variable flow, recharge, and complex structures— requires careful evaluation. However, the closed-system assumptions are often applied for the simplification of the case study.

Several field studies have explored how flow and mixing processes play an important role in nitrogen cycling in the aquifers. For example, (Well et al., 2010) examined N₂O isotopologue signatures ($\delta^{15}N$, $\delta^{18}O$, and $\delta^{15}N^{SP}$) in a sandy aquifer and observed near-complete N₂O reduction to N₂, attributing this to slow diffusion and limited N₂O escape in saturated groundwater- resulting

in isotopic signatures comparable to those seen in closed-system incubations. Similarly, (Weymann et al., 2008) observed N_2 and N_2O accumulation in nitrate-contaminated groundwater and studied changes in gas concentrations to estimate nitrate loss. Their mass balance calculations involved accumulation of gaseous denitrification products, assuming limited external exchange with surrounding water — effectively reflecting closed-system structure in specific aquifers. Further (Mander et al., 2014) applied isotopologue ratio analysis ($\delta^{15}N$, $\delta^{18}O$, and $\delta^{15}N^{SP}$) to evaluate denitrification in riparian alder forest aquifers. The study reported denitrification as the dominant nitrogen removal pathway and demonstrated substantial accumulation of N_2 and N_2O in water-saturated, low-oxygen zones. Although not explicitly studied as a closed system, the mass balance methodology assumed limited mixing and dilution during transformation processes. In another study, (Well et al., 2012) applied a closed-system nitrogen balance to estimate N_2O emissions. While the approach was based on the stoichiometric balance of nitrogen species to evaluate denitrification extent, the findings also indicated that recharge and groundwater mixing contributed to isotopic and concentration variability- indicating natural groundwater systems are only partly closed.

Collectively, these studies suggest that while certain aquifer zones— with low permeability or strong redox gradients—may exhibit reduction-dominated closed-system behavior, most groundwaters are not completely closed and are affected by water flow, mixing, and recharge. In our study, the use of low-level ^{15}N-labelling in a closed, suboxic incubation system enabled detailed analysis of nitrate reduction pathways in groundwater systems. However, real aquifer conditions—particularly affected by wastewater inputs or organic carbon—are more complex and may involve complex mixing and transport processes which can affect nitrogen transformation products. Therefore, even though closed-system lab incubations are useful for elucidating microbial nitrogen processes, their results should be supported by field measurements or transport models that better reflect the open and variable nature of groundwater systems.

5. Conclusions and outlook

This study demonstrates the intricate dynamics of N transformations in groundwater samples by integrating isotope analyses, microbial gene abundance, and FRAME modeling to elucidate the microbial mechanisms involved. Application of multi-compound isotope studies (NO_3^-, NO_2^-, N_2O) combined with the novel idea of low-level ^{15}N labelling and microbiome studies ~~provide~~provides a very detailed insight into the occurring processes and reveal some unexpected mechanisms. Based on this complex dataset we can document the co-occurrence of the oxidation and reduction pathways and existence of different, separated NO_2^- pools.

NO_2^- production is likely driven by nitrification processes linked to the oxidation of organic N from the elevated DON levels in water samples. Also, the data indicated the simultaneous

occurrence of denitrification processes, particularly under suboxic conditions induced during incubation, highlighting the dynamic nature of nitrogen cycling.

Isotope-based source partitioning in this study assumes a closed system approach. However, natural groundwater environments may often exhibit open-system behavior due to water movement, nutrient inflow, and microbial activity and therefore, the estimated source contributions- especially based on isotope mass balances and FRAME modeling are more representative for controlled laboratory conditions. Although tracer application and microbial data helped minimize uncertainties from concurrent processes such as DON oxidation or oxygen exchange, certain limitations still apply and require future field applications to validate closed-system approaches under varying conditions.

Future investigations into the role of DON could deepen understanding of its impact on nitrification and denitrification in waters. While this study focused on samples with elevated NO_3^-/DON concentrations to investigate nitrogen transformation processes, samples with higher NH_4^+ concentrations were not included in the incubation experiments as they typically showed low NO_3^- levels below detection limit for isotope analyses. As such, the role of NH_4^+ in NO_2^- formation under such conditions could not be evaluated in detail and requires further research. Broader application of these integrated methods combining isotope analyses and microbial gene studies in field-scale studies can improve monitoring and management of nitrogen pollution in groundwater systems.

6. Data availability

Original data are available in the zenodo repository files (https://zenodo.org/records/15076761). Material necessary for this study's findings is presented in the paper and in the appendix.

7. Author contribution

78. Competing interest

89. Financial support

1381

1382   ~~7~~

1383

1384

1385

10. References

Böhlke, J.K., Smith, R.L., Hannon, J.E., 2007. Isotopic Analysis of N and O in Nitrite and Nitrate by Sequential Selective Bacterial Reduction to N_2O. Anal Chem 79, 5888–5895. https://doi.org/10.1021/ac070176k

Boumaiza, L., Stotler, R.L., Mayer, B., Matiatos, I., Sacchi, E., Otero, N., Johannesson, K.H., Huneau, F., Chesnaux, R., Blarasin, M., Re, V., Knöller, K., 2024. How the $\delta^{18}O_{NO_3}$ versus $\delta^{15}N_{NO_3}$ Plot Can Be Used to Identify a Typical Expected Isotopic Range of Denitrification for NO_3-Impacted Groundwaters. ACS ES&T Water 4, 5243–5254. https://doi.org/10.1021/acsestwater.4c00796

Brettar, I., Sanchez-Perez, J.-M., Trémolières, M., 2002. Nitrate elimination by denitrification in hardwood forest soils of the Upper Rhine floodplain - Correlation with redox potential and organic matter. Hydrobiologia 469, 11–21. https://doi.org/10.1023/A:1015527611350

Broman, E., Zilius, M., Samuiloviene, A., Vybernaite-Lubiene, I., Politi, T., Klawonn, I., Voss, M., Nascimento, F.J.A., Bonaglia, S., 2021. Active DNRA and denitrification in oxic hypereutrophic waters. Water Res 194. https://doi.org/10.1016/j.watres.2021.116954

Bucha, M., Lewicka-Szczebak, D., Wójtowicz, P., 2025. Simultaneous measurement of greenhouse gases (CH4, CO2 and N2O) at atmospheric levels using a gas chromatography system. Atmos Meas Tech 1–16.

Buchen-Tschiskale, C., Well, R., Flessa, H., 2023. Tracing nitrogen transformations during spring development of winter wheat induced by 15N labeled cattle slurry applied with different techniques. Science of The Total Environment 871, 162061. https://doi.org/10.1016/j.scitotenv.2023.162061

Butterbach-Bahl, K., Baggs, E.M., Dannenmann, M., Kiese, R., Zechmeister-Boltenstern, S., 2013. Nitrous oxide emissions from soils: how well do we understand the processes

and their controls? Philosophical Transactions of the Royal Society B: Biological Sciences 368, 20130122. https://doi.org/10.1098/rstb.2013.0122

Chen, G., Zhao, W., Yang, Y., Chen, D., Wang, Y., Li, F., Zhao, Z., Cao, F., Liu, T., 2021. Chemodenitrification by Fe(II) and nitrite: Effects of temperature and dual N[sbnd]O isotope fractionation. Chem Geol 575. https://doi.org/10.1016/j.chemgeo.2021.120258

Clague, J.C., Stenger, R., Morgenstern, U., 2019. The influence of unsaturated zone drainage status on denitrification and the redox succession in shallow groundwater. Science of The Total Environment 660, 1232–1244. https://doi.org/10.1016/j.scitotenv.2018.12.383

Cui, Y.-X., Biswal, B.K., Guo, G., Deng, Y.-F., Huang, H., Chen, G.-H., Wu, D., 2019. Biological nitrogen removal from wastewater using sulphur-driven autotrophic denitrification. Appl Microbiol Biotechnol 103, 6023–6039. https://doi.org/10.1007/s00253-019-09935-4

Deb, S., Lewicka-Szczebak, D., Rohe, L., 2024. Microbial nitrogen transformations tracked by natural abundance isotope studies and microbiological methods: A review. Science of The Total Environment 926, 172073. https://doi.org/10.1016/j.scitotenv.2024.172073

Denk, T.R.A., Mohn, J., Decock, C., Lewicka-Szczebak, D., Harris, E., Butterbach-Bahl, K., Kiese, R., Wolf, B., 2017. The nitrogen cycle: A review of isotope effects and isotope modeling approaches. Soil Biol Biochem. https://doi.org/10.1016/j.soilbio.2016.11.015

Ding, B., Li, Z., Cai, M., Lu, M., Liu, W., 2022. Feammox is more important than anammox in anaerobic ammonium loss in farmland soils around Lake Taihu, China. Chemosphere 305, 135412. https://doi.org/10.1016/j.chemosphere.2022.135412

Einsiedl, F., Wunderlich, A., Sebilo, M., Coskun, Ö.K., Orsi, W.D., Mayer, B., 2020. Biogeochemical evidence of anaerobic methane oxidation and anaerobic ammonium oxidation in a stratified lake using stable isotopes. Biogeosciences 17, 5149–5161. https://doi.org/10.5194/bg-17-5149-2020

Espenberg, M., Pille, K., Yang, B., Maddison, M., Abdalla, M., Smith, P., Li, X., Chan, P.-L., Mander, Ü., 2024. Towards an integrated view on microbial CH4, N2O and N2 cycles in brackish coastal marsh soils: A comparative analysis of two sites. Science of The Total Environment 918, 170641. https://doi.org/10.1016/j.scitotenv.2024.170641

Espenberg, M., Truu, M., Mander, Ü., Kasak, K., Nõlvak, H., Ligi, T., Oopkaup, K., Maddison, M., Truu, J., 2018. Differences in microbial community structure and nitrogen cycling in natural and drained tropical peatland soils. Sci Rep 8, 4742. https://doi.org/10.1038/s41598-018-23032-yhttps://doi.org/10.1038/s41598-018-23032-y

Harris, S. J., Liisberg, J., Xia, L., Wei, J., Zeyer, K., Yu, L., Barthel, M., Wolf, B., Kelly, B. F. J., Cendón, D. I., Blunier, T., Six, J., and Mohn, J., 2020. N2O isotopocule measurements using laser spectroscopy: analyzer characterization and intercomparison, Atmos. Meas. Tech., 13, 2797–2831, https://doi.org/10.5194/amt-13-2797-2020.

Heil, J., Vereecken, H., Brüggemann, N., 2016. A review of chemical reactions of nitrification intermediates and their role in nitrogen cycling and nitrogen trace gas formation in soil. Eur J Soil Sci. https://doi.org/10.1111/ejss.12306

45

Hommes, N.G., Sayavedra-Soto, L.A., Arp, D.J., 2003. Chemolithoorganotrophic Growth of *Nitrosomonas europaea* on Fructose. J Bacteriol 185, 6809–6814. https://doi.org/10.1128/JB.185.23.6809-6814.2003

Hu, J., Tian, J., Deng, X., Liu, X., Zhou, F., Yu, J., Chi, R., Xiao, C., 2024. Heterotrophic nitrification processes driven by glucose and sodium acetate: New insights into microbial communities, functional genes and nitrogen metabolism from metagenomics and metabolomics. Bioresour Technol 408, 131226. https://doi.org/10.1016/j.biortech.2024.131226

Kendall, C., Aravena, R., 2000. Nitrate Isotopes in Groundwater Systems, in: Environmental Tracers in Subsurface Hydrology. Springer US, Boston, MA, pp. 261–297. https://doi.org/10.1007/978-1-4615-4557-6_9

Kendall, C., Elliott, E.M., Wankel, S.D., 2007. Tracing Anthropogenic Inputs of Nitrogen to Ecosystems, in: Stable Isotopes in Ecology and Environmental Science. Wiley, pp. 375–449. https://doi.org/10.1002/9780470691854.ch12

Kuusemets, L., Mander, Ü., Escuer-Gatius, J., Astover, A., Kauer, K., Soosaar, K., Espenberg, M., 2024. Interactions of fertilisation and crop productivity on soil nitrogen cycle microbiome and gas emissions. https://doi.org/10.5194/egusphere-2024-593

Levy-Booth, D.J., Prescott, C.E., Grayston, S.J., 2014. Microbial functional genes involved in nitrogen fixation, nitrification and denitrification in forest ecosystems. Soil Biol Biochem 75, 11–25. https://doi.org/10.1016/j.soilbio.2014.03.021

Lewicka-Szczebak, D., Jansen-Willems, A., Müller, C., Dyckmans, J., Well, R., 2021. Nitrite isotope characteristics and associated soil N transformations. Sci Rep 11, 5008. https://doi.org/10.1038/s41598-021-83786-w

Lewicka-Szczebak, D., Lewicki, M.P., Well, R., 2020. N2O isotope approaches for source partitioning of N2O production and estimation of N2O reduction – validation with the 15N gas-flux method in laboratory and field studies. Biogeosciences 17, 5513–5537. https://doi.org/10.5194/bg-17-5513-2020

Lewicki, M.P., Lewicka-Szczebak, D., Skrzypek, G., 2022. FRAME—Monte Carlo model for evaluation of the stable isotope mixing and fractionation. PLoS One 17, e0277204. https://doi.org/10.1371/journal.pone.0277204

Liu, R., Xia, L., Liu, M., Gao, Z., Feng, J., You, H., Qu, W., Xing, T., Wang, J., Zhao, Y., 2022. Influence of the carbon source concentration on the nitrate removal rate in groundwater. Environmental Technology (United Kingdom) 43, 3355–3365. https://doi.org/10.1080/09593330.2021.1921053

M. Sainju, U., Ghimire, R., P. Pradhan, G., 2020. Nitrogen Fertilization I: Impact on Crop, Soil, and Environment, in: Nitrogen Fixation. IntechOpen. https://doi.org/10.5772/intechopen.86028

Mander, Ü., Well, R., Weymann, D., Soosaar, K., Maddison, M., Kanal, A., Lõhmus, K., Truu, J., Augustin, J., Tournebize, J., 2014. Isotopologue ratios of N2O and N2 measurements underpin the importance of denitrification in differently N-loaded riparian alder forests. Environ Sci Technol 48, 11910–11918. https://doi.org/10.1021/es501727h

MASTA, M., ESPENBERG, M., KUUSEMETS, L., PÄRN, J., THAYAMKOTTU, S., SEPP, H., KIRSIMÄE, K., SGOURIDIS, F., KASAK, K., SOOSAAR, K., MANDER, Ü., 2024. 15N tracers and microbial analyses reveal in situ N2O sources in contrasting water regimes of a drained peatland forest. Pedosphere 34, 749–758. https://doi.org/10.1016/j.pedsph.2023.06.006

Mohn, J., Wolf, B., Toyoda, S., Lin, C.T., Liang, M.C., Brüggemann, N., Wissel, H., Steiker, A.E., Dyckmans, J., Szwec, L., Ostrom, N.E., Casciotti, K.L., Forbes, M., Giesemann, A., Well, R., Doucett, R.R., Yarnes, C.T., Ridley, A.R., Kaiser, J., Yoshida, N., 2014. Interlaboratory assessment of nitrous oxide isotopomer analysis by isotope ratio mass spectrometry and laser spectroscopy: Current status and perspectives. Rapid Communications in Mass Spectrometry 28, 1995–2007. https://doi.org/10.1002/rcm.6982

Moore, K.B., Ekwurzel, B., Esser, B.K., Hudson, G.B., Moran, J.E., 2006. Sources of groundwater nitrate revealed using residence time and isotope methods. Applied Geochemistry 21, 1016–1029. https://doi.org/10.1016/j.apgeochem.2006.03.008

Mosley, O.E., Gios, E., Close, M., Weaver, L., Daughney, C., Handley, K.M., 2022. Nitrogen cycling and microbial cooperation in the terrestrial subsurface. ISME Journal 16, 2561–2573. https://doi.org/10.1038/s41396-022-01300-0

Müller, C., Laughlin, R.J., Spott, O., Rütting, T., 2014. Quantification of N2O emission pathways via a 15N tracing model. Soil Biol Biochem 72, 44–54. https://doi.org/10.1016/j.soilbio.2014.01.013

Müller, C., Stevens, R.J., Laughlin, R.J., 2004. A 15N tracing model to analyse N transformations in old grassland soil. Soil Biol Biochem 36, 619–632. https://doi.org/10.1016/j.soilbio.2003.12.006

Nikolenko, O., Jurado, A., Borges, A. V., Knöller, K., Brouyère, S., 2018. Isotopic composition of nitrogen species in groundwater under agricultural areas: A review. Science of the Total Environment. https://doi.org/10.1016/j.scitotenv.2017.10.086

Olichwer, T., Wcisło, M., Staśko, S., Buczyński, S., Modelska, M., Tarka, R., 2012. ~~Numerical Model Of The Catchments Of The Oziąbel And Wołczyński Strumień Rivers-Wołczyn Municipality~~NUMERICAL MODEL OF THE CATCHMENTS OF THE OZIĄBEL AND WOŁCZYŃSKI STRUMIEŃ RIVERS-WOŁCZYN MUNICIPALITY, Studia Geotechnica et Mechanica.

Rohe, L., Oppermann, T., Well, R., Horn, M.A., 2020. Nitrite induced transcription of p450nor during denitrification by Fusarium oxysporum correlates with the production of N2O with a high 15N site preference. Soil Biol Biochem 151, 108043. https://doi.org/10.1016/j.soilbio.2020.108043

Rütting, T., Aronsson, H., Delin, S., 2018. Efficient use of nitrogen in agriculture. Nutr Cycl Agroecosyst. https://doi.org/10.1007/s10705-017-9900-8

Rütting, T., Müller, C., 2008. Process-specific analysis of nitrite dynamics in a permanent grassland soil by using a Monte Carlo sampling technique. Eur J Soil Sci 59, 208–215. ~~https://doi.org/10.1111/j.1365-2389.2007.00976.x~~https://doi.org/10.1111/j.1365-2389.2007.00976.x

~~Sainju, M., U., Ghimire, R., P. Pradhan, G., 2020. Nitrogen Fertilization I: Impact on Crop, Soil, and Environment, in: Nitrogen Fixation. IntechOpen. https://doi.org/10.5772/intechopen.86028~~

Sigman, D.M., Casciotti, K.L., Andreani, M., Barford, C., Galanter, M., Böhlke, J.K., 2001. A bacterial method for the nitrogen isotopic analysis of nitrate in seawater and freshwater. Anal Chem 73, 4145–4153. https://doi.org/10.1021/ac010088e

Wang, P., Li, J.L., Luo, X.Q., Ahmad, M., Duan, L., Yin, L.Z., Fang, B.Z., Li, S.H., Yang, Y., Jiang, L., Li, W.J., 2022. Biogeographical distributions of nitrogen-cycling

functional genes in a subtropical estuary. Funct Ecol 36, 187–201. https://doi.org/10.1111/1365-2435.13949

Wang, X., Wells, N.S., Xiao, W., Hamilton, J.L., Jones, A.M., Collins, R.N., 2022. Mackinawite (FeS) Chemodenitrification of Nitrate (NO_3^-) under Acidic to Neutral pH Conditions and Its Stable N and O Isotope Dynamics. ACS Earth Space Chem 6, 2801–2811. https://doi.org/10.1021/acsearthspacechem.2c00158

Ward, M., Jones, R., Brender, J., De Kok, T., Weyer, P., Nolan, B., Villanueva, C., Van Breda, S., 2018. Drinking Water Nitrate and Human Health: An Updated Review. Int J Environ Res Public Health 15, 1557. https://doi.org/10.3390/ijerph15071557

Watanabe, Y., Aoki, W., Ueda, M., 2023. Ammonia Production Using Bacteria and Yeast toward a Sustainable Society. Bioengineering 10, 82. https://doi.org/10.3390/bioengineering10010082

Wei, J., Ibraim, E., Brüggemann, N., Vereecken, H., Mohn, J., 2019. First real-time isotopic characterisation of N2O from chemodenitrification. Geochim Cosmochim Acta 267, 17–32. https://doi.org/10.1016/j.gca.2019.09.018

Well, R., Buchen-Tschiskale, C., Burbank, J., Dannenmann, M., Lewicka-Szczebak, D., Mohn, J., Rohe, L., Scheer, C., Tuzzeo, S., Wolf, B., 2025. Production of standard gases for routine calibration of stable isotope ratios of N2 and N2O https://doi.org/10.5194/egusphere-egu24-11996

Well, R., Burkart, S., Giesemann, A., Grosz, B., Köster, J.R., Lewicka-Szczebak, D., 2019. Improvement of the ^{15}N gas flux method for *in situ* measurement of soil denitrification and its product stoichiometry. Rapid Communications in Mass Spectrometry 33, 437–448. https://doi.org/10.1002/rcm.8363

Well, R., Eschenbach, W., Flessa, H., von der Heide, C., Weymann, D., 2012. Are dual isotope and isotopomer ratios of N 2O useful indicators for N 2O turnover during denitrification in nitrate-contaminated aquifers? Geochim Cosmochim Acta 90, 265–282. https://doi.org/10.1016/j.gca.2012.04.045

Well, R., Weymann, D., Kahle, P., Maddison, M., Mander, Ü., Soosaar, K., Flessa, H., 2010. Isotopologue signatures of N2O from groundwater, tile drainage water, riparian wetlands and waste water treatment wetlands, Geophysical Research Abstracts.

Weymann, D., Well, R., Flessa, H., Von Der Heide, C., Deurer, M., Meyer, K., Konrad, C., Walther, W., 2008. Groundwater N 2 O emission factors of nitrate-contaminated aquifers as derived from denitrification progress and N 2 O accumulation, Biogeosciences.

Wolters, T., Bach, T., Eisele, M., Eschenbach, W., Kunkel, R., McNamara, I., Well, R., Wendland, F., 2022. The derivation of denitrification conditions in groundwater: Combined method approach and application for Germany. Ecol Indic 144, 109564. https://doi.org/10.1016/J.ECOLIND.2022.109564

Yu, L., Harris, E., Lewicka-Szczebak, D., Barthel, M., Blomberg, M.R.A., Harris, S.J., Johnson, M.S., Lehmann, M.F., Liisberg, J., Müller, C., Ostrom, N.E., Six, J., Toyoda, S., Yoshida, N., Mohn, J., 2020. What can we learn from N 2 O isotope data? – Analytics, processes and modelling. Rapid Communications in Mass Spectrometry 34. https://doi.org/10.1002/rcm.8858

Zhang, Y., Cai, Z., Zhang, J., Müller, C., 2023. The controlling factors and the role of soil heterotrophic nitrification from a global review. Applied Soil Ecology 182, 104698. https://doi.org/10.1016/j.apsoil.2022.104698

Zheng, J., Fujii, K., Koba, K., Wanek, W., Müller, C., Jansen-Willems, A.B., Nakajima, Y., Wagai, R., Canarini, A., 2023. Revisiting process-based simulations of soil nitrite dynamics: Tighter cycling between nitrite and nitrate than considered previously. Soil Biol Biochem 178, 108958. https://doi.org/10.1016/j.soilbio.2023.108958

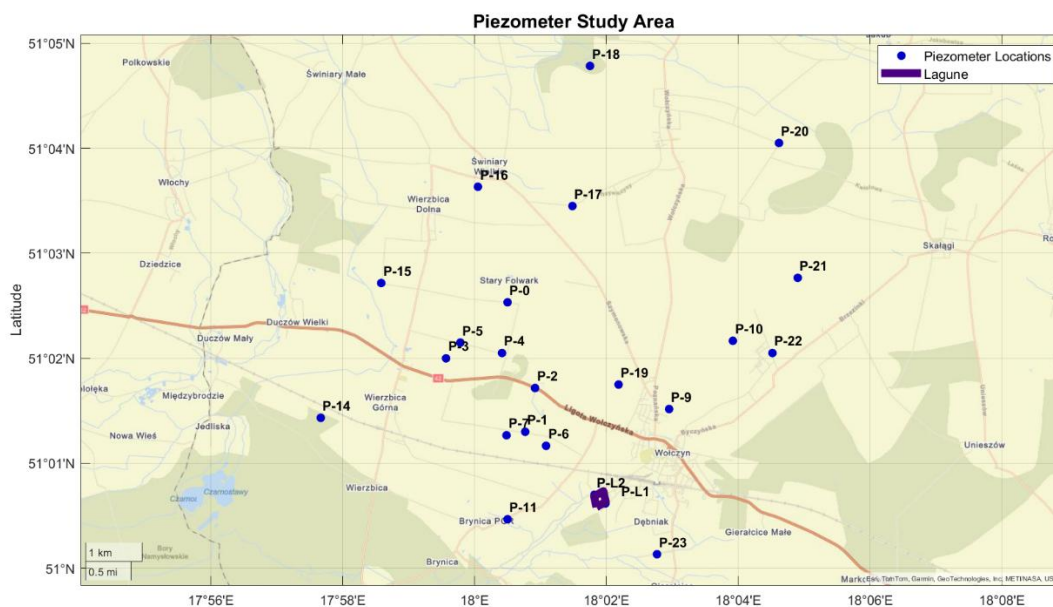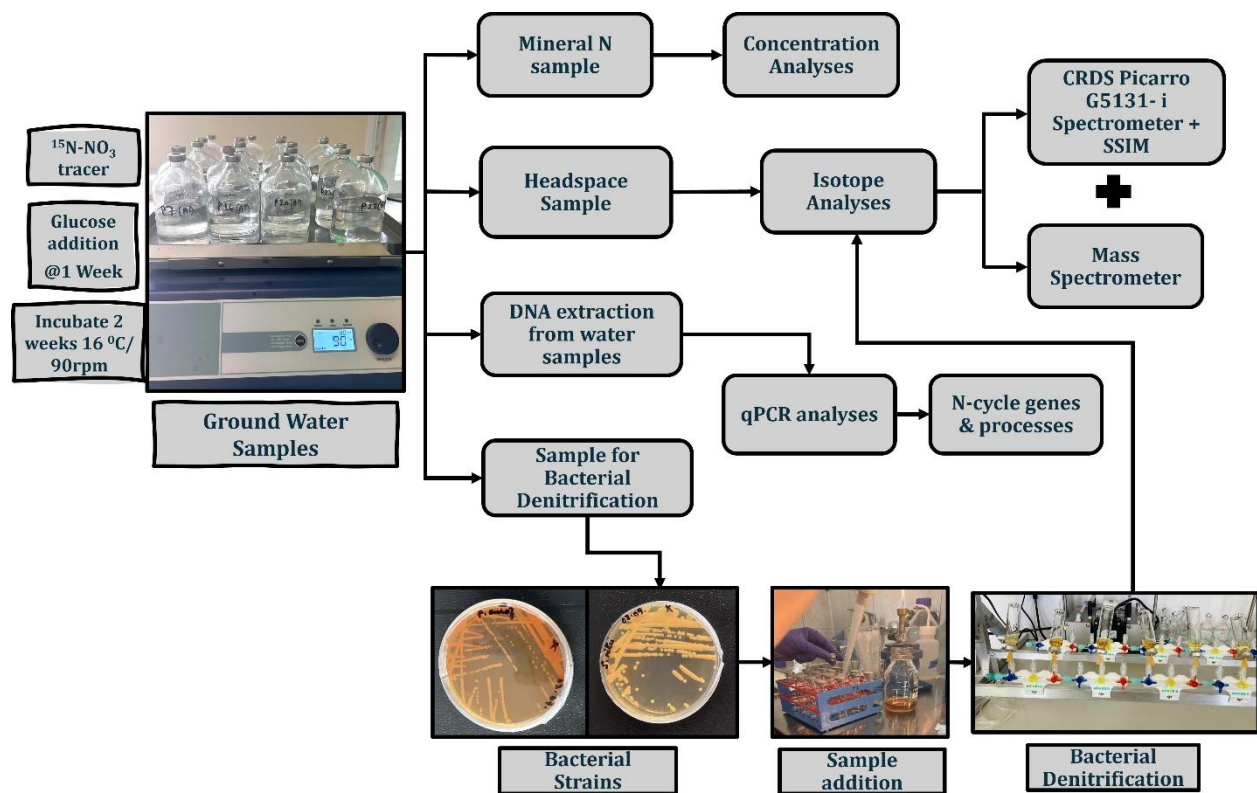Zhu-Barker, X., Cavazos, A.R., Ostrom, N.E., Horwath, W.R., Glass, J.B., 2015. The importance of abiotic reactions for nitrous oxide production. Biogeochemistry 126, 251–267. https://doi.org/10.1007/s10533-015-0166-4

Figure 1: Piezometer Study Area near Wołczyn, Poland (Purple-marked area indicates the lagune for yeast-production sewage storage).

Figure 2: Experimental Setup for microbial analyses (qPCR, Groundwater Incubation) and Isotopic Analysis.

50

A

B
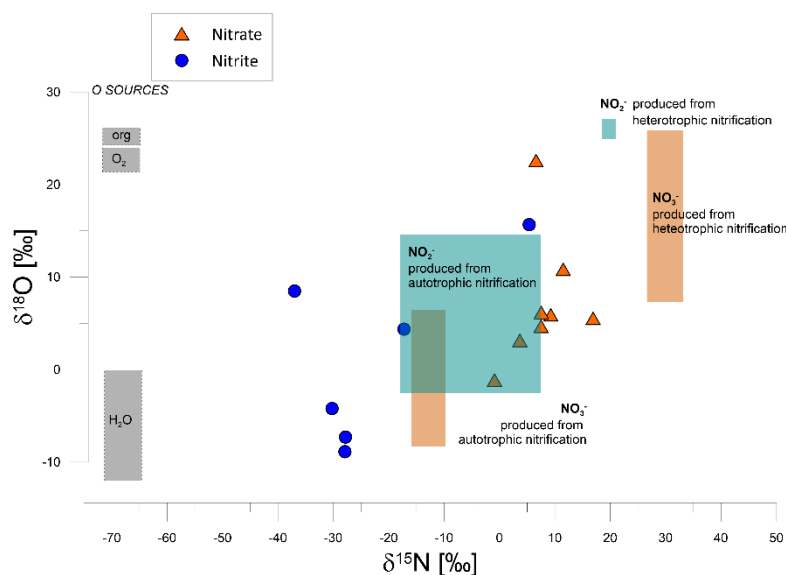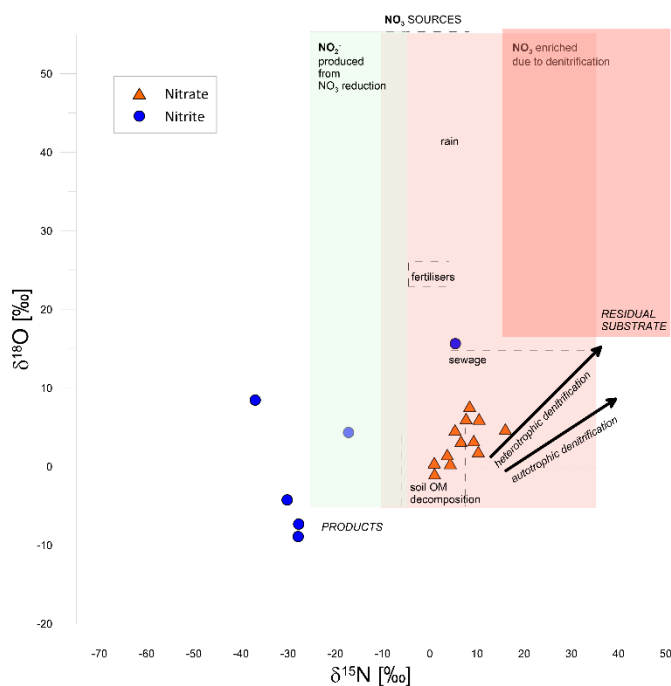
Figure 3Figure 3: The isotope signatures of NO_3^- (orange triangles) and NO_2^- (blue circles) in field groundwater samples presented with the literature data for particular N sources and isotope effects for main N transformations, with respect to denitrification processes (A) and nitrification nitrite and nitrate sources (B).
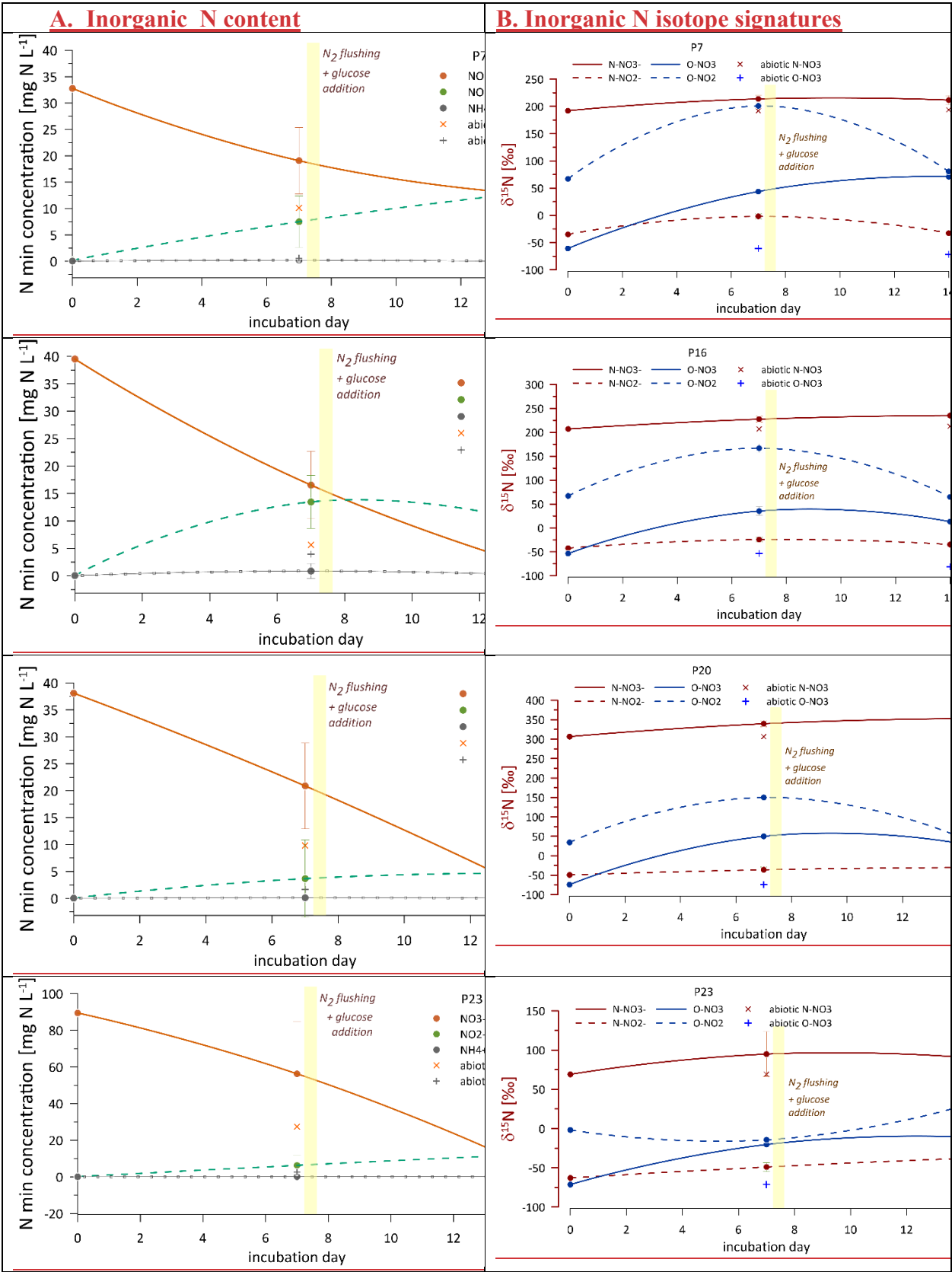
A. Inorganic N content

B. Inorganic N isotope signatures

1607
1608
1609
1610
1611
1612

Figure 4: Content of inorganic nitrogen forms (orange line: NO₃⁻, green line: NO₂⁻, grey line: NH₄⁺) (A) and their isotopic signatures (δ¹⁵N and δ¹⁸O) , (B) during laboratory incubation.

Table 1: Inputs and results of the mass balance calculations for determining the contribution of nitrate reduction (NAR) in the nitrite pool

Piezometer	$\Delta\delta^{15}N_{NO_2}$	$\delta^{15}N_{NO3-0}$	NAR [%]	Δ [NO₂-] mg N L^{-1}	mg L^{-1} NAR	Δ [NO₃-] mg N L^{-1}
P-7	33.1	192.2	17.2	7.3	1.3	-13.7
P-16	18.1	207.1	8.7	13.4	1.2	-23.0
P-20	13.4	306.5	4.4	3.6	0.2	-17.2
P-23	14.1	69.0	20.4	6.1	1.2	-33.2

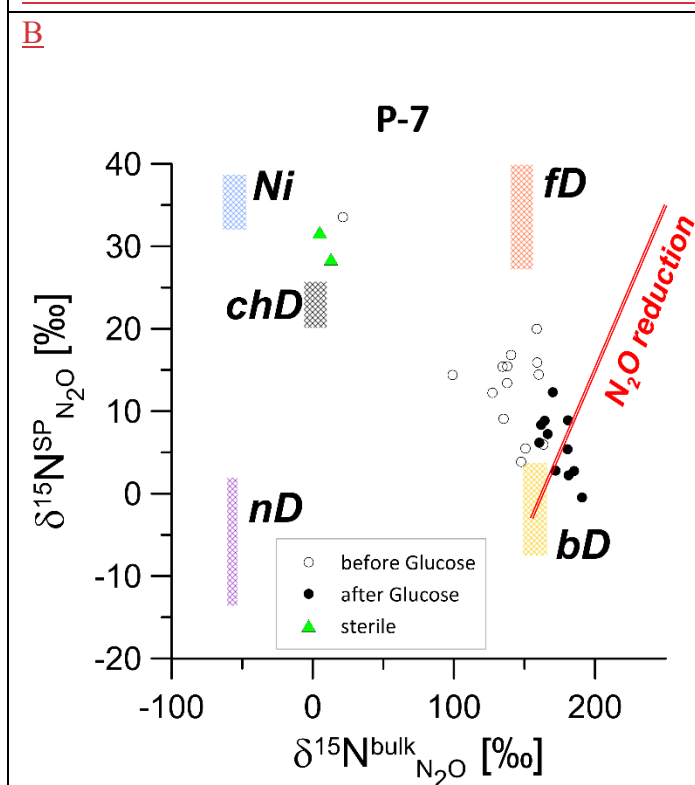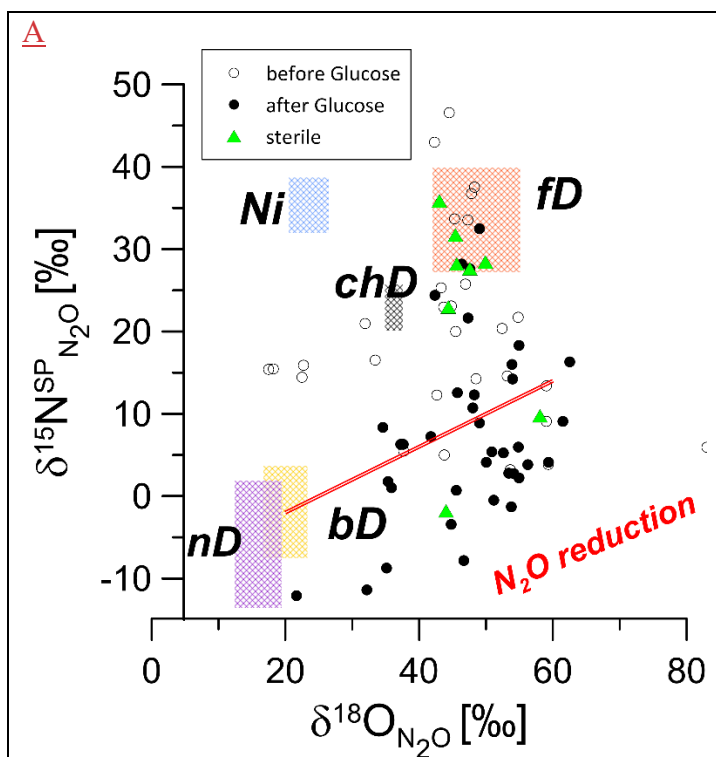**Figure 5:Isotopic Signatures of Nitrite (NO₂⁻) during laboratory Incubation: first phase, before glucose addition: empty circles, second phase, after glucose addition: filled circles.**
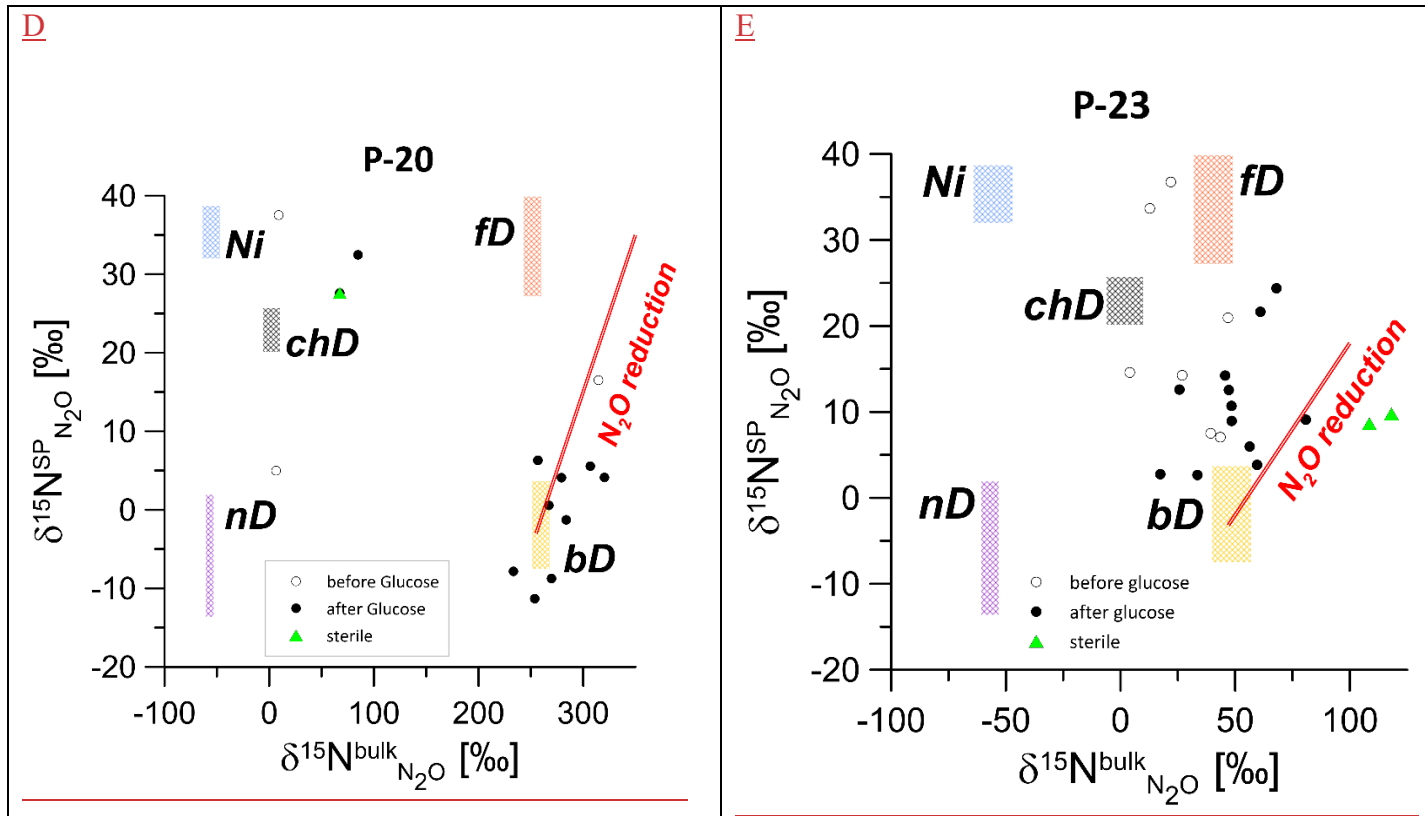
1622
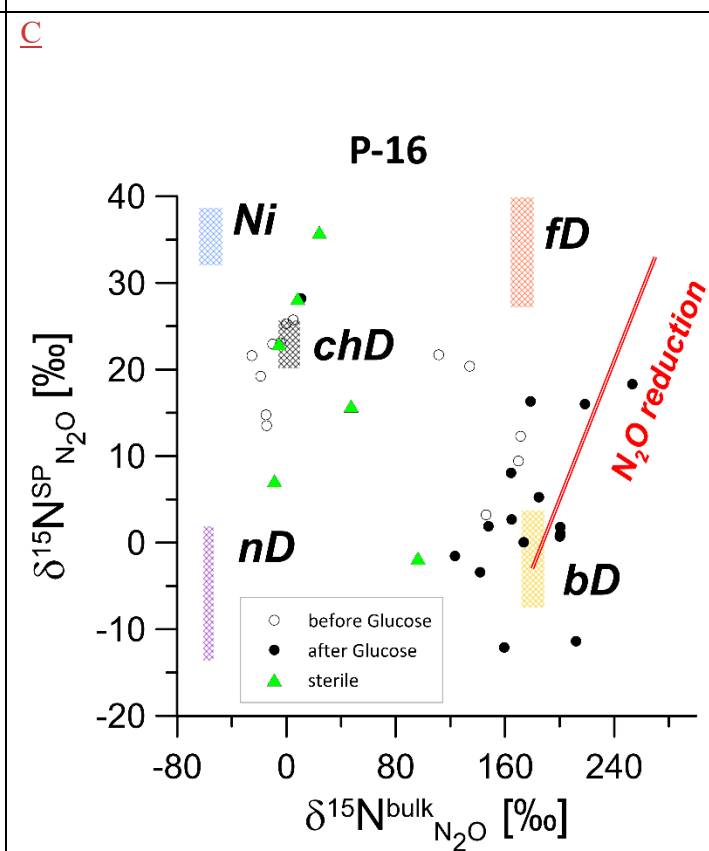
Figure 6: Isotopic signatures ($\delta^{15}N^{SP}_{N2O}$, $\delta^{18}O_{N2O}$ and $\delta^{15}N_{N2O}$) highlighting N₂O dynamics and microbial nitrogen transformation pathways during laboratory incubation for groundwater samples (P, abbreviated for piezometer: P-7, P-16, P-20, and P-23).
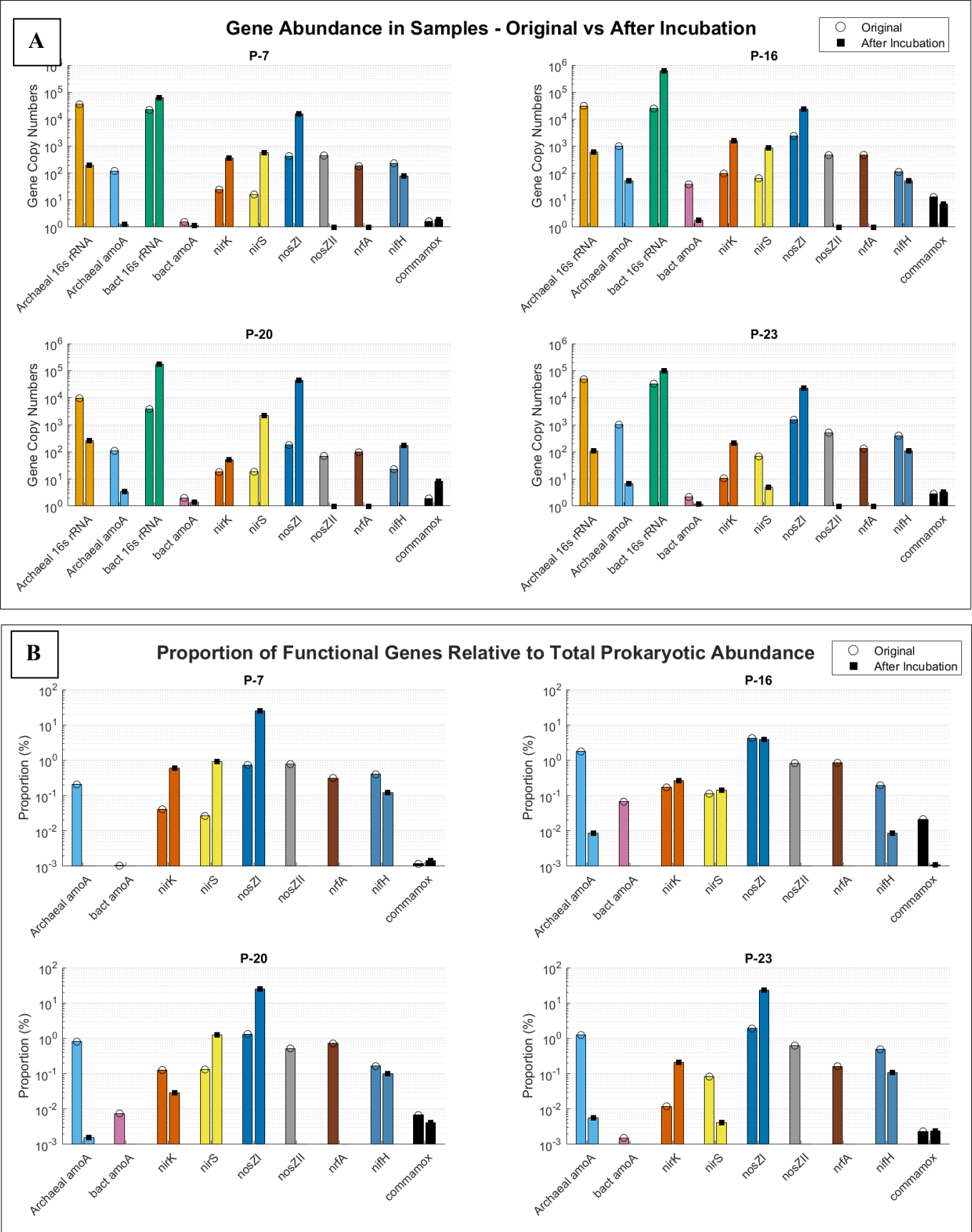
Figure 7: Microbial Functional Gene Dynamics in Groundwater Samples (A) Comparison of gene abundance in groundwater samples and (B) Functional Gene Proportions in samples before and after incubation

1627